Appendix I

Time Domain Simulations

I.1 Pitch Control Input Analysis

Simulations were performed with the gull-wing mathematical model in order to investigate pitch control input response. The damping, control authority and static margin of the model were varied to investigate the effect on the aircraft step response. The simulations of the pitch control input analysis differs from the gull wing sensitivity analysis (Section 5.4) in the sense that only one parameter value was changed in isolation in the case of the sensitivity study. In reality many of the parameters of the aircraft model have coupling effects with other parameters. A change in the CG, for example, has an influence on the aerodynamic pitch damping coefficient (C_{M_q})[1]. With the gull wing sensitivity analysis other parameters such as damping were held constant while CG was varied in order to investigate the effect and sensitivity of each parameter on the aircraft dynamics in isolation. With the pitch control input analysis the influence of parameter changes on other parameters was included in the simulation models.

The aircraft mathematical models were subjected to elevon step inputs (-1 degree, resulting in nose up rotation) during simulation runs.

A matrix of different aircraft configurations was defined for the use of

[1]The change in magnitude of pitch damping coefficient with a change in CG is not negligible in the case of tailless aircraft.

UNIVERSITEIT VAN PRETORIA
UNIVERSITY OF PRETORIA
YUNIBESITHI YA PRETORIA

the pitch control input analysis. Each of the configurations was used in a simulation with an elevon step input. Inertia was kept constant at the baseline value for all configurations, because it was shown in Chapter 5 that a change in pitch inertia does not have a sufficiently large influence on the aircraft response.

The control authority was varied in the following ways: For one set of model configurations the control authority was 20% higher than the baseline and for the other the control authority was 20% lower than the baseline. The third model configuration had the baseline control authority.

The model parameter values for aerodynamic damping were varied as follows: A baseline damping configuration was used for one set of simulations. A configuration with 20% higher damping than the baseline configuration was used for another set of simulations and a configuration with 20% lower damping than the baseline configuration was used for yet another set of simulations.

The static margin was varied in the following ways for the different aircraft mathematical models used in the different simulations to provide the following configurations:

- 2% at 30° sweep
- 5% at 30° sweep
- 10.7% at 30° sweep
- 15% at 30° sweep

The static margin is specified at a certain sweep angle, because static margin is a function of the sweep angle of the outboard wing.

The variations of parameters were not implemented on the mathematical models in isolation of other parameters, as was the case with the sensitivity analysis of Chapter 5. In other words, if the static margin changed, the damping also changed along with the elevon control authority.

The control authority simulations were performed for the following values of wing sweep:

UNIVERSITEIT VAN PRETORIA
UNIVERSITY OF PRETORIA
YUNIBESITHI YA PRETORIA

- 20° sweep
- 24° sweep
- 30° sweep
- 36° sweep

The parameter variations described here lead to a matrix of 144 aircraft configurations. The simulation schedule for the different models is noted in Appendix H. Each simulation configuration for the pitch response analysis is numbered there and the numbering system will be used to refer to the configurations and associated simulation results. The simulation results for all the configurations are not all displayed in this section or the rest of the document. The following simulation results were chosen for inclusion in the document:

- All static margin variations at 30° sweep having the baseline aerodynamic damping and control authority. (Configurations 81, 90, 99, 108) Only this set of configurations is plotted in the main document, while the other sets are documented in this Appendix. Baseline values refer to the calculated model parameter values as presented in Section 4.7.
- All static margin variations at 24° sweep having the baseline aerodynamic damping and control authority. (Configurations 45, 54, 63, 72. Configurations 45 and 54 are statically unstable and therefore no results are plotted)
- All static margin variations at 36° sweep having the baseline aerodynamic damping and control authority. (Configurations 117, 126, 135, 144)
- All control authority variations at 30° sweep with the baseline aerodynamic damping at a 10.7% (at 30°) static margin configuration. (Configurations 93, 96, 99)

UNIVERSITEIT VAN PRETORIA
UNIVERSITY OF PRETORIA
YUNIBESITHI YA PRETORIA

- All control authority variations at 24° sweep with the baseline aerodynamic damping at a 10.7% (at 30°) static margin configuration. (Configurations 57, 60, 63)
- All damping variations at 30° sweep with the baseline control authority at a 10.7% (at 30°) static margin configuration. (Configurations 97, 98, 99)

The results of the first item are presented in this section. The rest are shown in Appendix I.2. All the results are discussed here.

The simulations shown here were performed with a step input as described in Section 4.8.2.

The time domain simulations predictably show that higher control authority leads to a more rapid initial aircraft response. Lower static margins show higher magnitude pitch responses than higher static margins. The higher pitch responses are accompanied by high pitch rates and normal accelerations.

Damping decreases the magnitude of the pitch response and makes the pitching moment less rapid. Damping has a smaller effect on the natural frequency of the aircraft modes than static margin.

The pitch step responses of the different gull-wing configurations are oscillatory in nature. The phugoid mode is not strongly damped. The step response is similar in shape to the step response of the SB-13 aircraft shown in Mönnich & Dalldorff (1993:349). The aircraft tends to pitch down after the initial upward pitching motion, even though the control input is held constant.

Configuration 45 was statically unstable. The simulation response of this configuration is not shown because it was divergent. This type of configuration needs to be investigated with controller (pilot) in the loop study. The pilot or controller may prevent a divergent response.

α, θ, pitch rate, normal acceleration and speed versus time were plotted as the output of this investigation. These parameters were chosen because they are most important for studying the aircraft modes. The normal acceleration is included because it is used in the calculation of the C-star response. Pitch

UNIVERSITEIT VAN PRETORIA
UNIVERSITY OF PRETORIA
YUNIBESITHI YA PRETORIA

rate and normal acceleration have a large influence on the pilot opinion of an aircraft configuration.

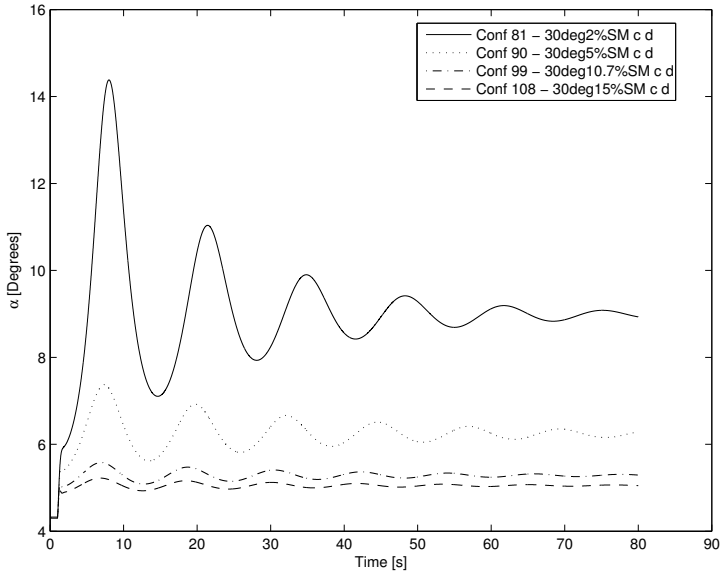

Figure I.1: Response in aircraft angle of attack (α) to a unit step elevon control input for 30° outboard wing sweep at different static margins with the baseline control authority and aerodynamic damping.

UNIVERSITEIT VAN PRETORIA
UNIVERSITY OF PRETORIA
YUNIBESITHI YA PRETORIA

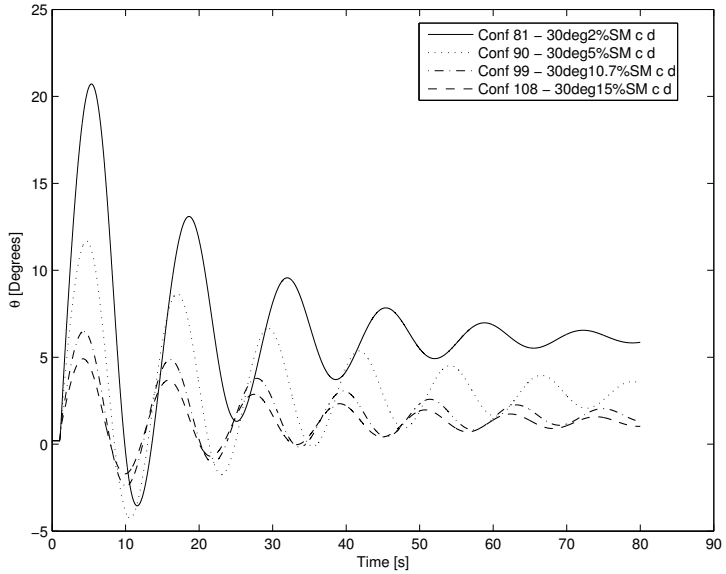

Figure I.2: Response in aircraft attitude (θ) to a unit step elevon control input to a unit step elevon control input for 30° outboard wing sweep at different static margins with the baseline control authority and aerodynamic damping.

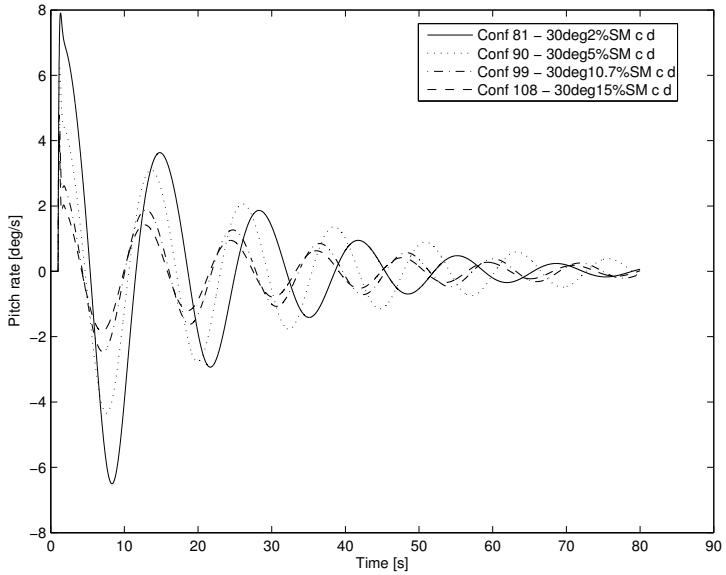

Figure I.3: Response in aircraft pitch rate to a unit step elevon control input for 30° outboard wing sweep at different static margins with the baseline control authority and aerodynamic damping.

UNIVERSITEIT VAN PRETORIA
UNIVERSITY OF PRETORIA
YUNIBESITHI YA PRETORIA

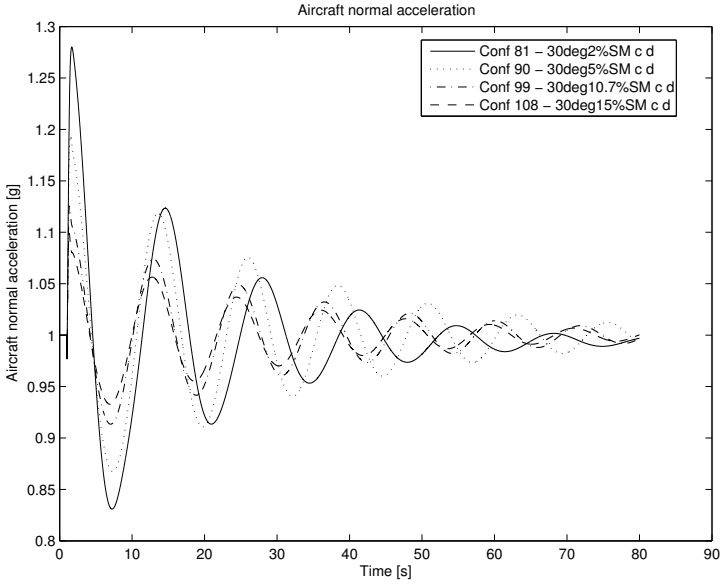

Figure I.4: Response in aircraft normal acceleration to a unit step elevon control input for 30° outboard wing sweep at different static margins with the baseline control authority and aerodynamic damping.

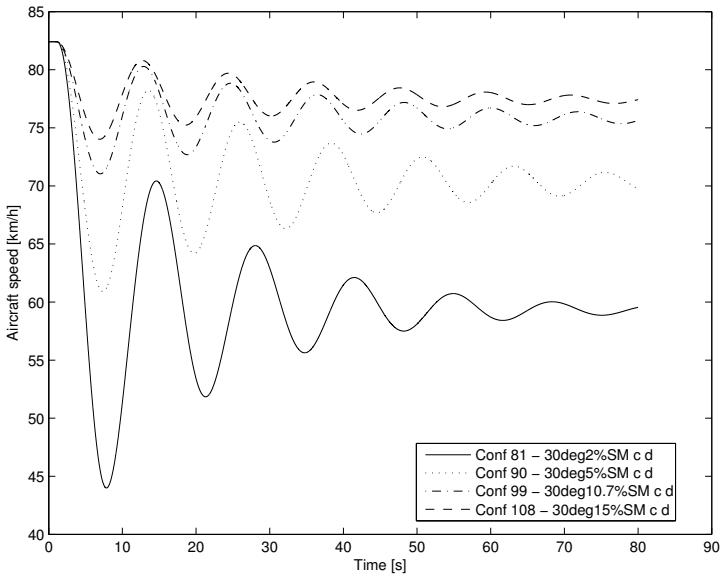

Figure I.5: Response in aircraft airspeed to a unit step elevon control input for 30° outboard wing sweep at different static margins with the baseline control authority and aerodynamic damping.

UNIVERSITEIT VAN PRETORIA
UNIVERSITY OF PRETORIA
YUNIBESITHI YA PRETORIA

I.2 Pitch Control Input Simulations

I.2.1 Configurations 45, 54, 63, 72

Simulation results of all static margin variations at 24° sweep having the baseline aerodynamic damping and control authority. (Configurations 45 (unstable, not plotted), 54, 63, 72)

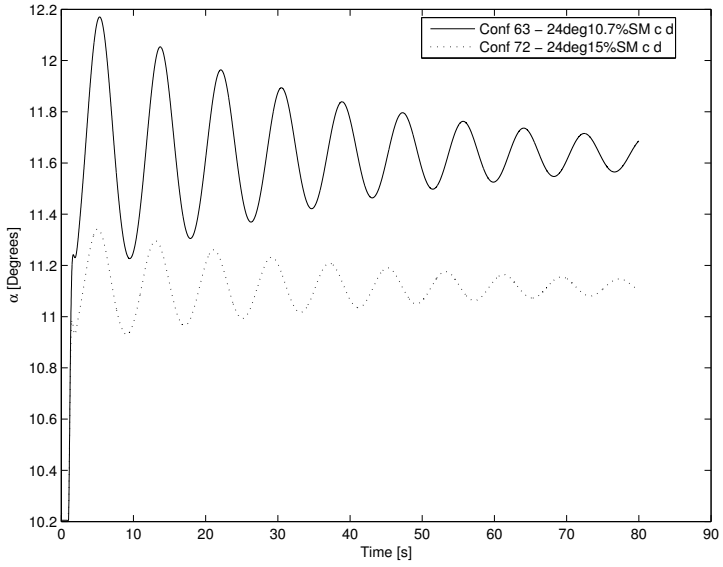

Figure I.6: Response in aircraft angle of attack (α) to a unit step elevon control input for 24° outboard wing sweep at different static margins with the baseline control authority and aerodynamic damping.

UNIVERSITEIT VAN PRETORIA
UNIVERSITY OF PRETORIA
YUNIBESITHI YA PRETORIA

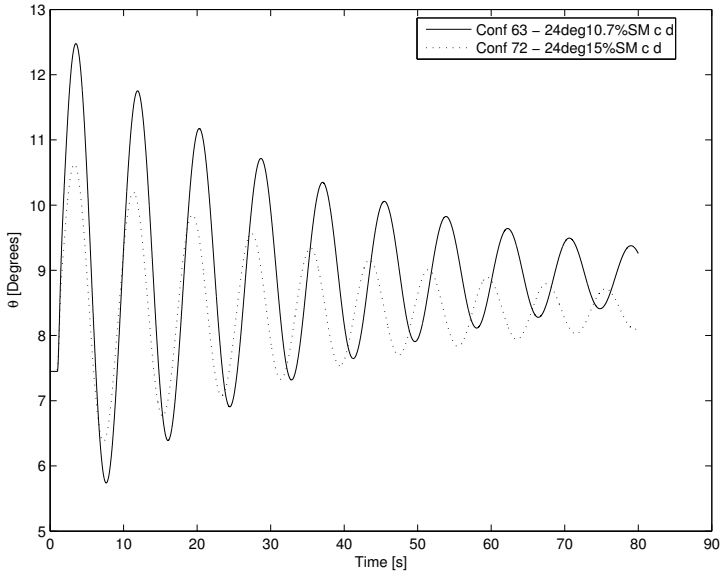

Figure I.7: Response in aircraft attitude (θ) to a unit step elevon control input for 24° outboard wing sweep at different static margins with the baseline control authority and aerodynamic damping.

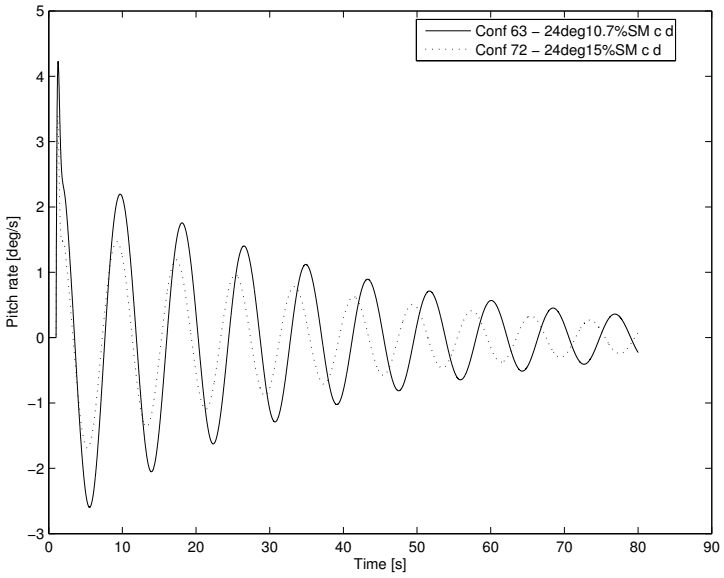

Figure I.8: Response in aircraft pitch rate to a unit step elevon control input for 24° outboard wing sweep at different static margins with the baseline control authority and aerodynamic damping.

UNIVERSITEIT VAN PRETORIA
UNIVERSITY OF PRETORIA
YUNIBESITHI YA PRETORIA

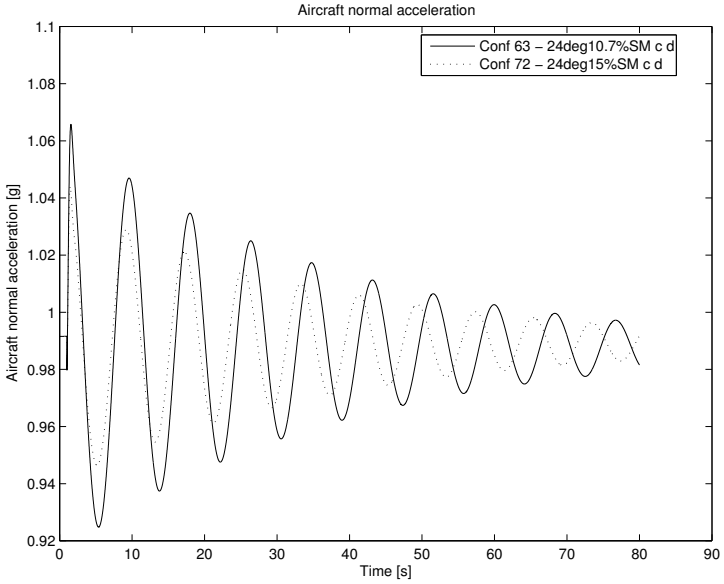

Figure I.9: Response in aircraft normal acceleration to a unit step elevon control input for 24° outboard wing sweep at different static margins with the baseline control authority and aerodynamic damping.

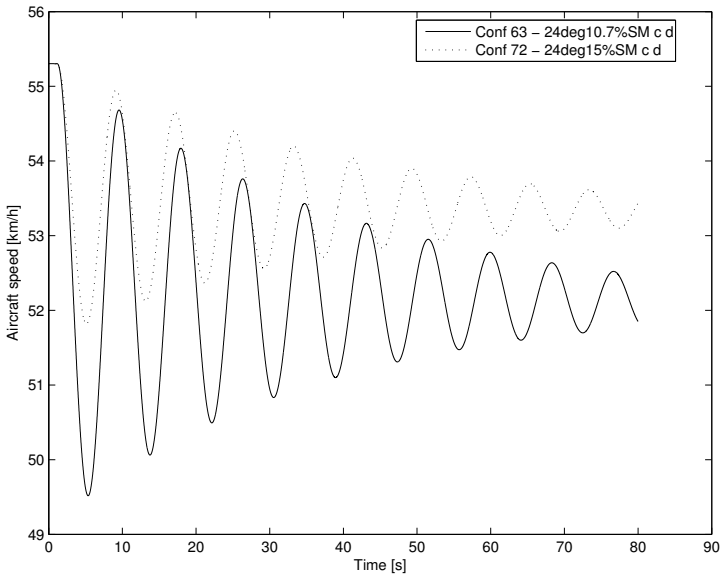

Figure I.10: Response in aircraft airspeed to a unit step elevon control input for 24° outboard wing sweep at different static margins with the baseline control authority and aerodynamic damping.

UNIVERSITEIT VAN PRETORIA
UNIVERSITY OF PRETORIA
YUNIBESITHI YA PRETORIA

I.2.2 Configurations 117, 126, 135, 144

Simulation results of all static margin variations at 36° sweep having the baseline aerodynamic damping and control authority. (Configurations 117, 126, 135, 144)

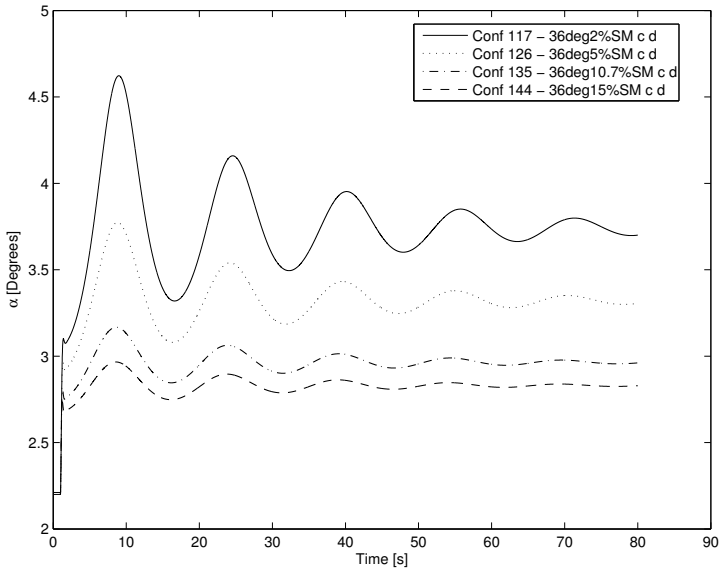

Figure I.11: Response in aircraft angle of attack (α) to a unit step elevon control input for 36° outboard wing sweep at different static margins with the baseline control authority and aerodynamic damping.

UNIVERSITEIT VAN PRETORIA
UNIVERSITY OF PRETORIA
YUNIBESITHI YA PRETORIA

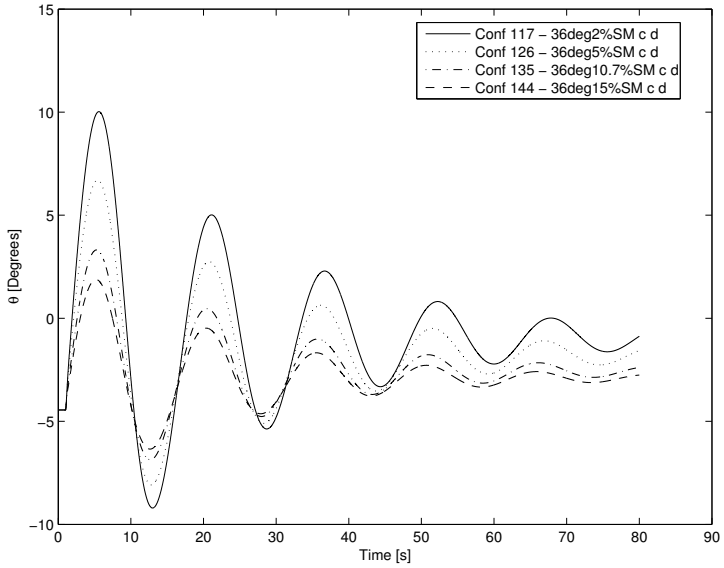

Figure I.12: Response in aircraft attitude (θ) to a unit step elevon control input for 36° outboard wing sweep at different static margins with the baseline control authority and aerodynamic damping.

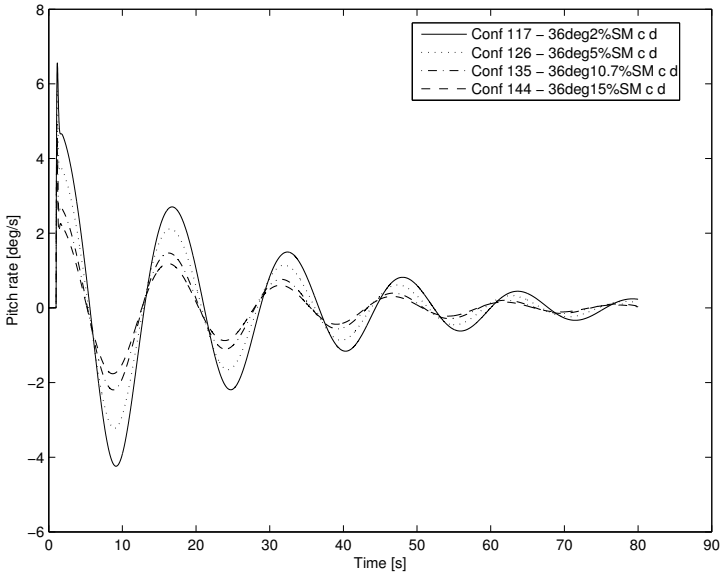

Figure I.13: Response in aircraft pitch rate to a unit step elevon control input for 36° outboard wing sweep at different static margins with the baseline control authority and aerodynamic damping.

UNIVERSITEIT VAN PRETORIA
UNIVERSITY OF PRETORIA
YUNIBESITHI YA PRETORIA

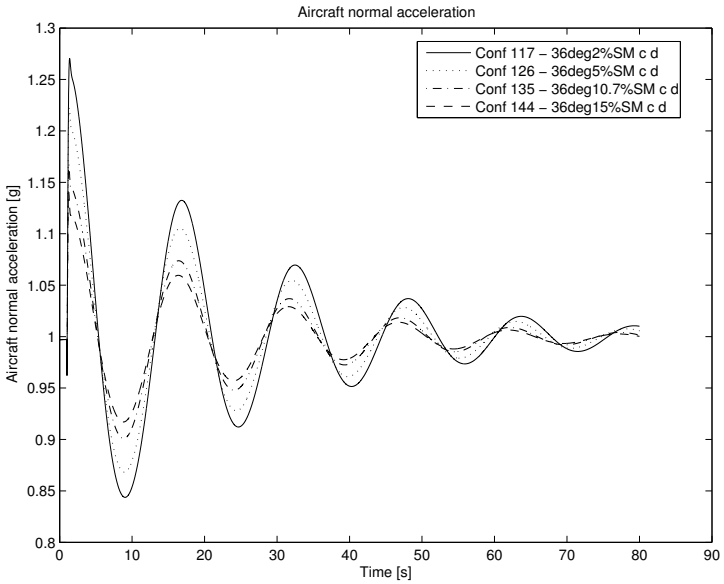

Figure I.14: Response in aircraft normal acceleration to a unit step elevon control input for 36° outboard wing sweep at different static margins with the baseline control authority and aerodynamic damping.

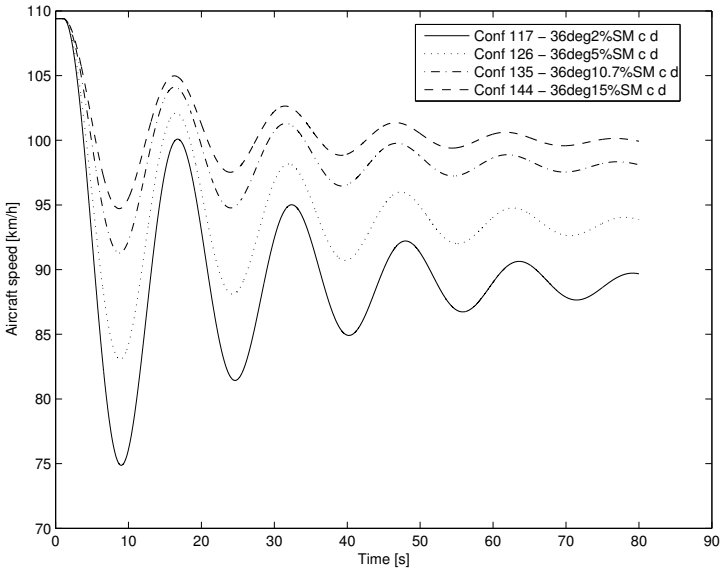

Figure I.15: Response in aircraft airspeed to a unit step elevon control input for 36° outboard wing sweep at different static margins with the baseline control authority and aerodynamic damping.

UNIVERSITEIT VAN PRETORIA
UNIVERSITY OF PRETORIA
YUNIBESITHI YA PRETORIA

I.2.3 Configurations 93, 96, 99

Simulation results of all control authority variations at 30° sweep with the baseline aerodynamic damping at a 10.7% (at 30°) static margin configuration. (Configurations 93, 96, 99)

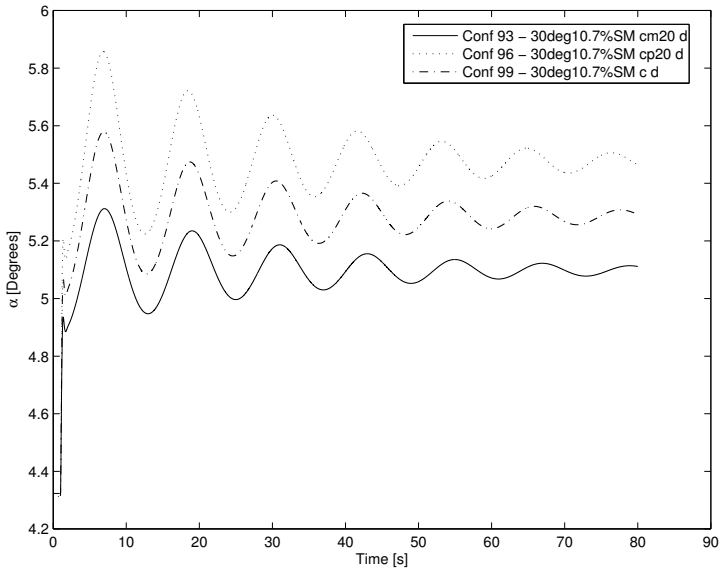

Figure I.16: Response in aircraft angle of attack (α) to a unit step elevon control input for 30° outboard wing sweep at a 10.7% static margin (at 30°) with the baseline aerodynamic damping with variations in control authority.

UNIVERSITEIT VAN PRETORIA
UNIVERSITY OF PRETORIA
YUNIBESITHI YA PRETORIA

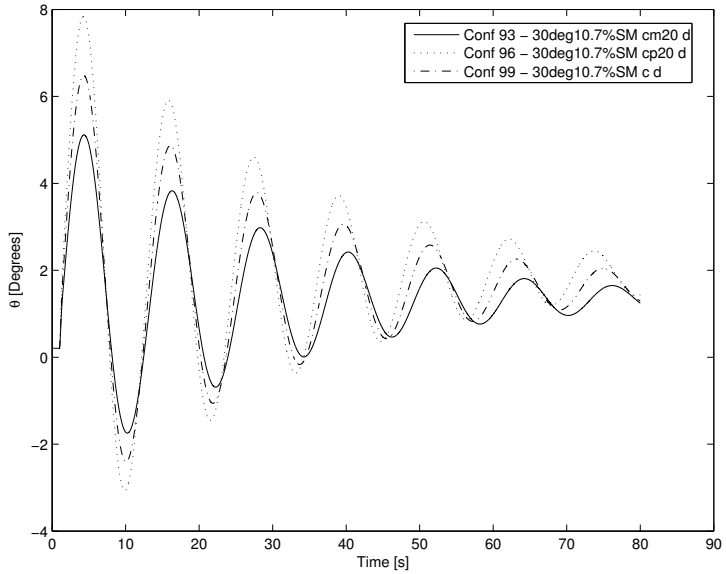

Figure I.17: Response in aircraft attitude (θ) to a unit step elevon control input for 30° outboard wing sweep at a 10.7% static margin (at 30°) with the baseline aerodynamic damping with variations in control authority.

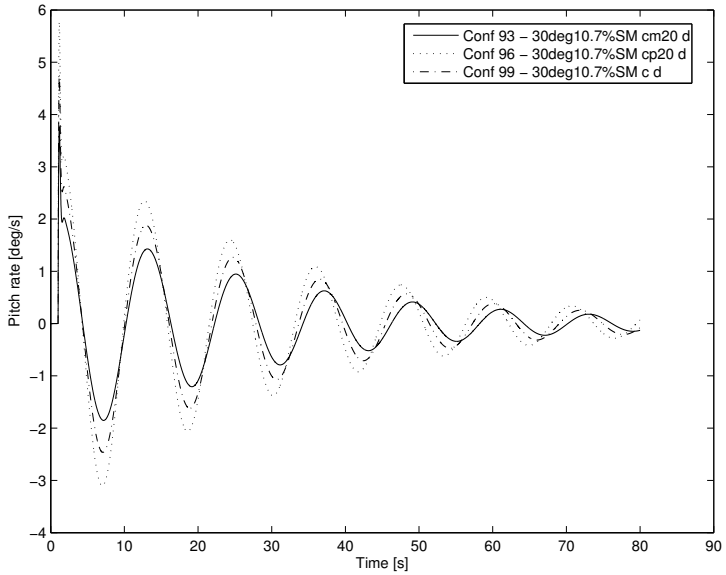

Figure I.18: Response in aircraft pitch rate to a unit step elevon control input for 30° outboard wing sweep at a 10.7% static margin (at 30°) with the baseline aerodynamic damping with variations in control authority.

UNIVERSITEIT VAN PRETORIA
UNIVERSITY OF PRETORIA
YUNIBESITHI YA PRETORIA

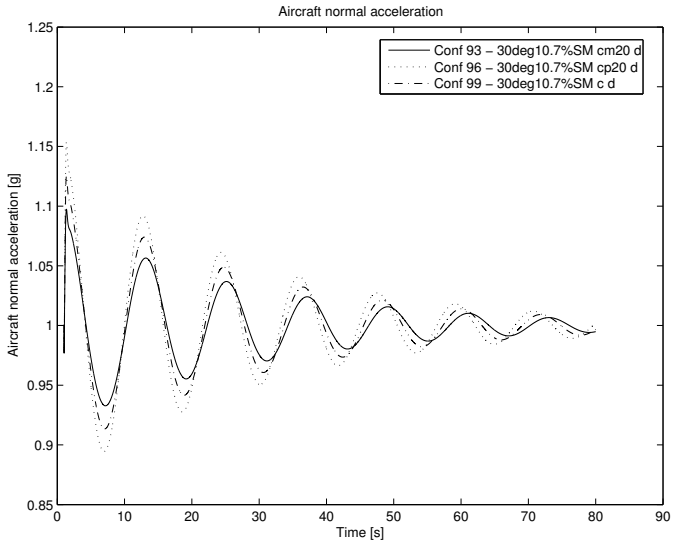

Figure I.19: Response in aircraft normal acceleration to a unit step elevon control input for 30° outboard wing sweep at a 10.7% static margin (at 30°) with the baseline aerodynamic damping with variations in control authority.

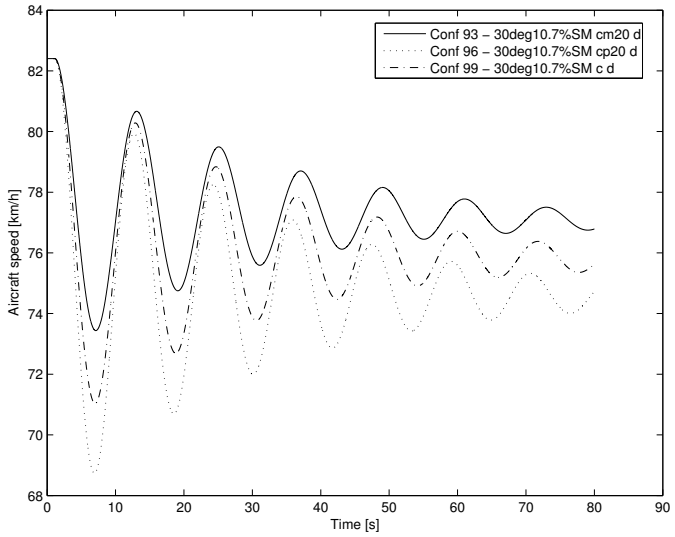

Figure I.20: Response in aircraft airspeed to a unit step elevon control input for 30° outboard wing sweep at a 10.7% static margin (at 30°) with the baseline aerodynamic damping with variations in control authority.

UNIVERSITEIT VAN PRETORIA
UNIVERSITY OF PRETORIA
YUNIBESITHI YA PRETORIA

I.2.4 Configurations 57, 60, 63

Simulation results of all control authority variations at 24° sweep with the baseline aerodynamic damping at a 10.7% (at 30°) static margin configuration. (Configurations 57, 60, 63)

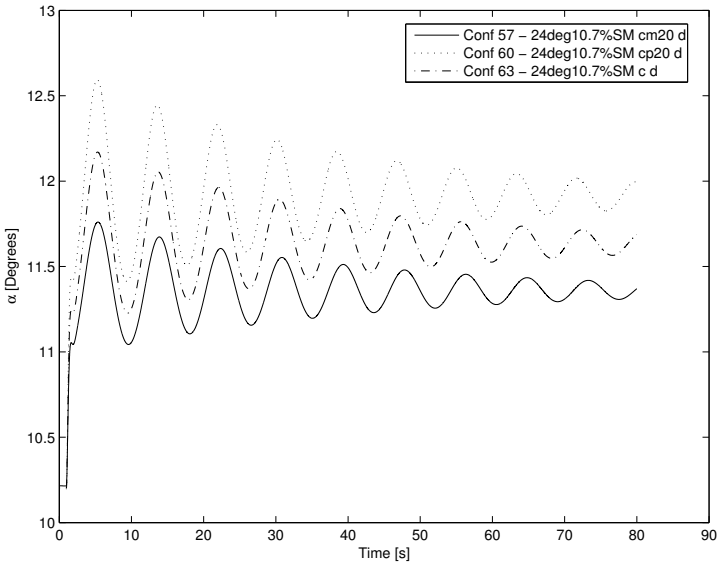

Figure I.21: Response in aircraft angle of attack (α) to a unit step elevon control input for 24° outboard wing sweep at a 10.7% static margin (at 30°) with the baseline aerodynamic damping with variations in control authority.

UNIVERSITEIT VAN PRETORIA
UNIVERSITY OF PRETORIA
YUNIBESITHI YA PRETORIA

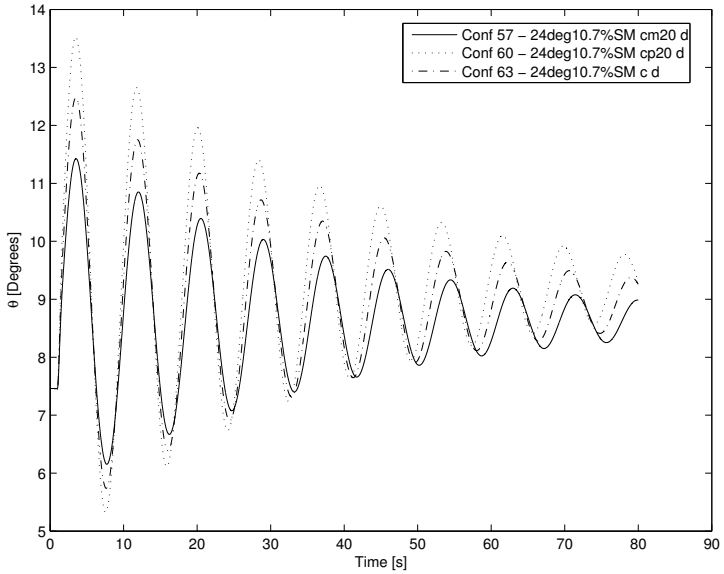

Figure I.22: Response in aircraft attitude (θ) to a unit step elevon control input for 24° outboard wing sweep at a 10.7% static margin (at 30°) with the baseline aerodynamic damping with variations in control authority.

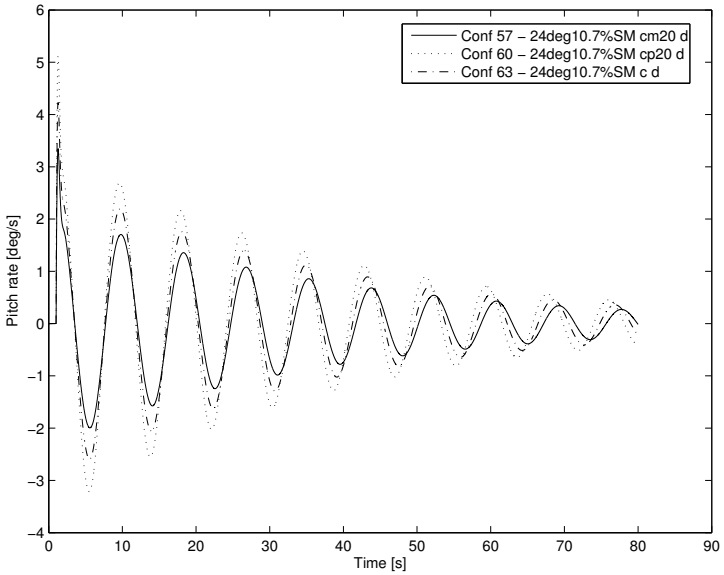

Figure I.23: Response in aircraft pitch rate to a unit step elevon control input for 24° outboard wing sweep at a 10.7% static margin (at 30°) with the baseline aerodynamic damping with variations in control authority.

UNIVERSITEIT VAN PRETORIA
UNIVERSITY OF PRETORIA
YUNIBESITHI YA PRETORIA

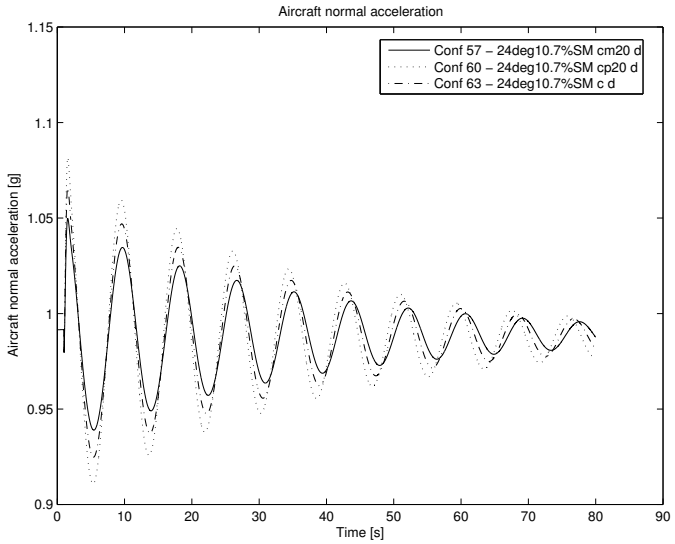

Figure I.24: Response in aircraft normal acceleration to a unit step elevon control input for 24° outboard wing sweep at a 10.7% static margin (at 30°) with the baseline aerodynamic damping with variations in control authority.

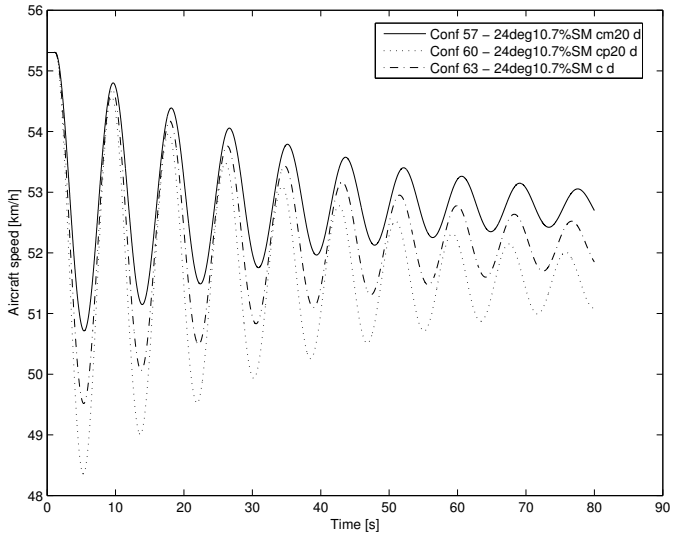

Figure I.25: Response in aircraft airspeed to a unit step elevon control input for 24° outboard wing sweep at a 10.7% static margin (at 30°) with the baseline aerodynamic damping with variations in control authority.

UNIVERSITEIT VAN PRETORIA
UNIVERSITY OF PRETORIA
YUNIBESITHI YA PRETORIA

I.2.5 Configurations 97, 98, 99

Simulation results of all damping variations at 30° sweep with the baseline control authority at a 10.7% (at 30°) static margin configuration. (Configurations 97, 98, 99)

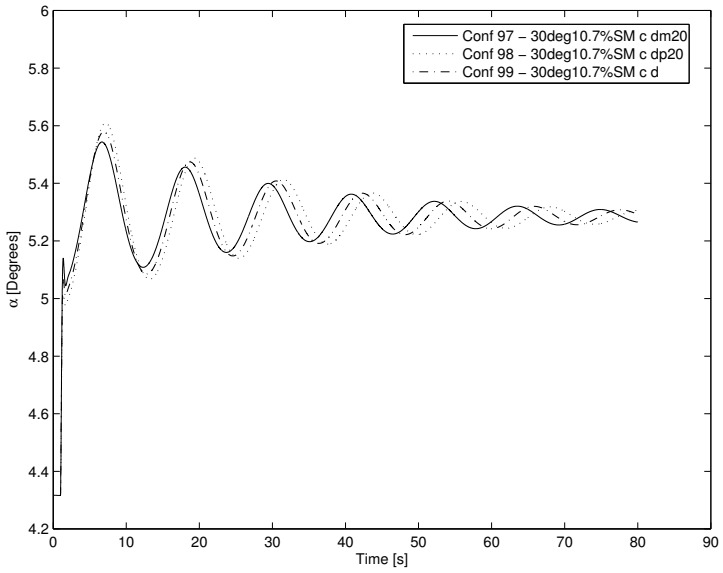

Figure I.26: Response in aircraft angle of attack (α) to a unit step elevon control input for 30° outboard wing sweep at a 10.7% static margin (at 30°) with the baseline control authority with variations in aerodynamic damping.

UNIVERSITEIT VAN PRETORIA
UNIVERSITY OF PRETORIA
YUNIBESITHI YA PRETORIA

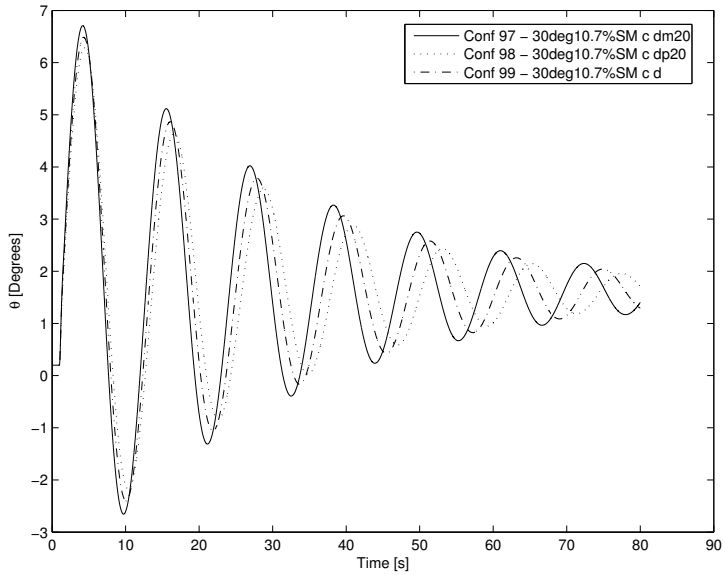

Figure I.27: Response in aircraft attitude (θ) to a unit step elevon control input for 30° outboard wing sweep at a 10.7% static margin (at 30°) with the baseline control authority with variations in aerodynamic damping.

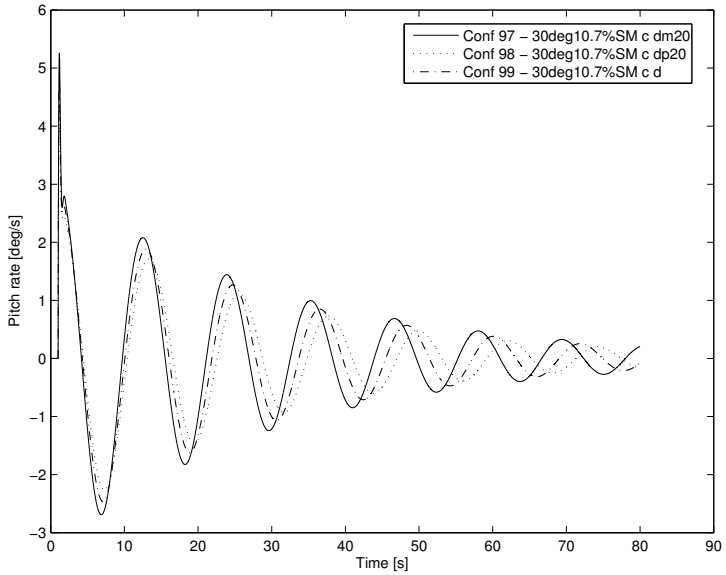

Figure I.28: Response in aircraft pitch rate to a unit step elevon control input for 30° outboard wing sweep at a 10.7% static margin (at 30°) with the baseline control authority with variations in aerodynamic damping.

UNIVERSITEIT VAN PRETORIA
UNIVERSITY OF PRETORIA
YUNIBESITHI YA PRETORIA

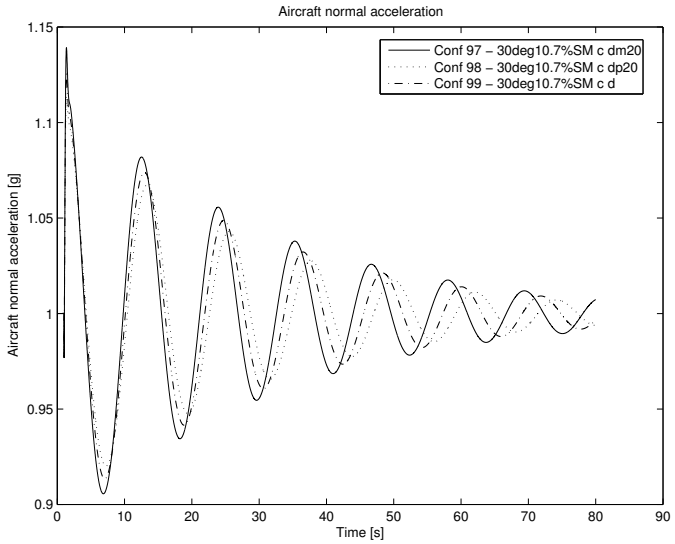

Figure I.29: Response in aircraft normal acceleration to a unit step elevon control input for 30° outboard wing sweep at a 10.7% static margin (at 30°) with the baseline control authority with variations in aerodynamic damping.

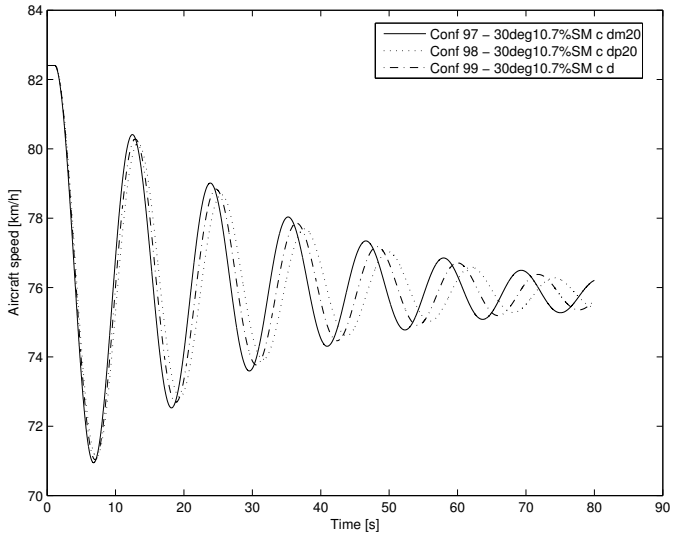

Figure I.30: Response in aircraft airspeed to a unit step elevon control input for 30° outboard wing sweep at a 10.7% static margin (at 30°) with the baseline control authority with variations in aerodynamic damping.

UNIVERSITEIT VAN PRETORIA
UNIVERSITY OF PRETORIA
YUNIBESITHI YA PRETORIA

I.3 Gust Response Analysis

Simulations were performed in order to investigate gust response of the gull-wing configuration. The mathematical models of the aircraft which represented different aircraft configurations were subjected to a vertical gust of type $1 - \cos$ with a peak value of 2 m/s that was introduced 1 second following the start of the simulation. A graphical representation of the gust is shown in Figure 4.13.

It is necessary to perform a study with respect to gust response since an aircraft might have satisfactory handling qualities in calm atmosphere, whilst having unpleasant handling qualities in rough air as shown in Chalk (1963) and Mönnich & Dalldorff (1993).

The static margin, outboard wing sweep and damping parameter values of the gull-wing configuration mathematical model were varied for the purposes of investigating the effects of these changes on the gust response of the aircraft. The static margin and aerodynamic damping parameters were varied in the same way as described in the pitch response analysis of Section I.1. All the gust response simulations were performed with the control input assumed to be fixed.

The numbering system used for the aircraft configurations of the gust response study is different from that of the pitch control study. The aircraft configurations of the gust response analysis is defined in Table H.2 of Appendix H. All the simulation results for the gust response study are not shown in this document. The gust response simulation results of the following configurations were chosen to be shown here:

- All static margin variations at 30° sweep having the baseline aerodynamic damping. (Configurations 27, 30, 33, 36)
- All static margin variations at 24° sweep having the baseline aerodynamic damping. (Configurations 15, 18, 21, 24)
- All static margin variations at 36° sweep having the baseline aerodynamic damping. (Configurations 39, 42, 45, 48)

UNIVERSITEIT VAN PRETORIA
UNIVERSITY OF PRETORIA
YUNIBESITHI YA PRETORIA

- All damping variations at 30° sweep at a 10.7% (at 30°) static margin configuration. (Configurations 31, 32, 33)

Only the responses of the first item are presented in this section (Figures I.31 to I.35). The responses of the other configurations described in the above list are shown in Appendix I.4 but are discussed here.

The following observations were made regarding the simulation results: Configuration 15 is statically unstable and therefore the simulation results with this configuration are not plotted.

Changes in static margin have a large influence on the magnitude of the aircraft pitch response and the natural frequencies of the aircraft modes. The simulated aircraft responses indicate that the low static margin configurations have smaller magnitudes and lower natural frequencies than the high static margin configurations.

The simulations with variations in damping showed that the damping influences the natural frequency as well as the damping of the aircraft response. The effect of damping is less significant than that of static margin.

UNIVERSITEIT VAN PRETORIA
UNIVERSITY OF PRETORIA
YUNIBESITHI YA PRETORIA

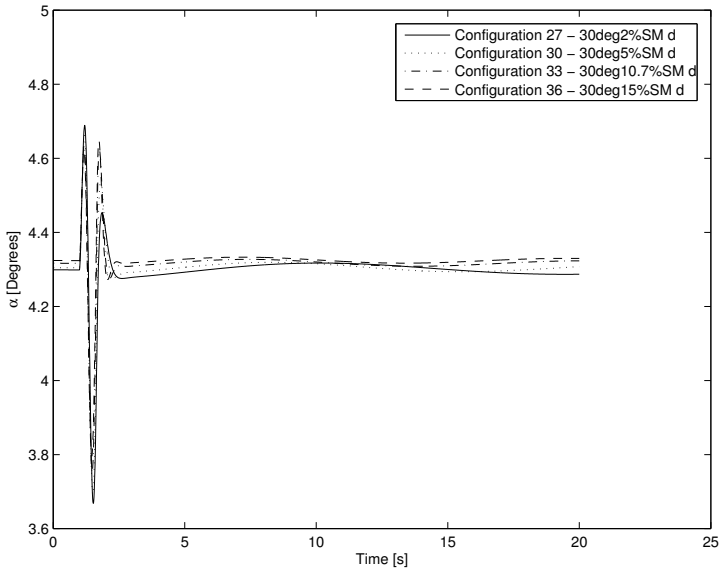

Figure I.31: Gust response for aircraft angle of attack (α) for 30° outboard wing sweep at different static margins with the baseline aerodynamic damping.

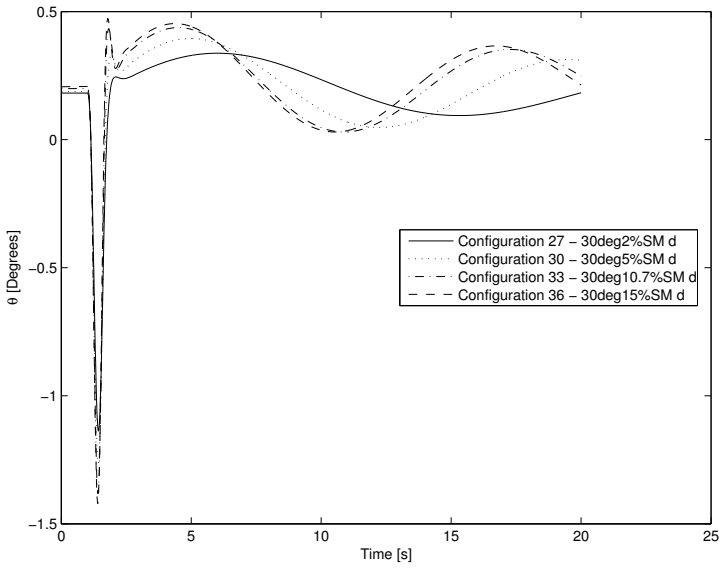

Figure I.32: Gust response for aircraft attitude (θ) for 30° outboard wing sweep at different static margins with the baseline aerodynamic damping.

UNIVERSITEIT VAN PRETORIA
UNIVERSITY OF PRETORIA
YUNIBESITHI YA PRETORIA

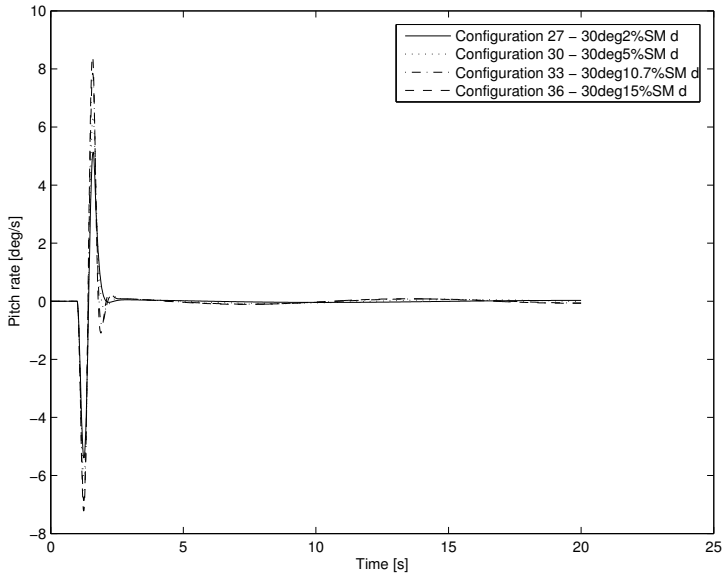

Figure I.33: Gust response for aircraft pitch rate for 30° outboard wing sweep at different static margins with the baseline aerodynamic damping.

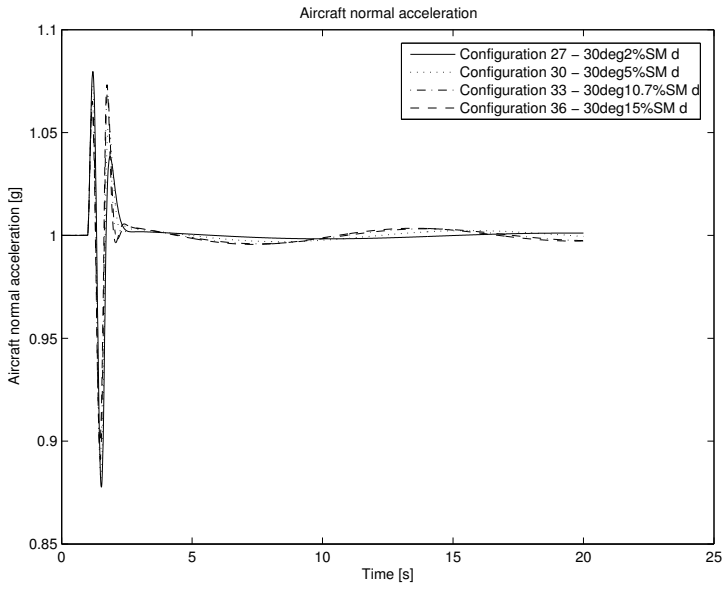

Figure I.34: Gust response for aircraft normal acceleration for 30° outboard wing sweep at different static margins with the baseline aerodynamic damping.

UNIVERSITEIT VAN PRETORIA
UNIVERSITY OF PRETORIA
YUNIBESITHI YA PRETORIA

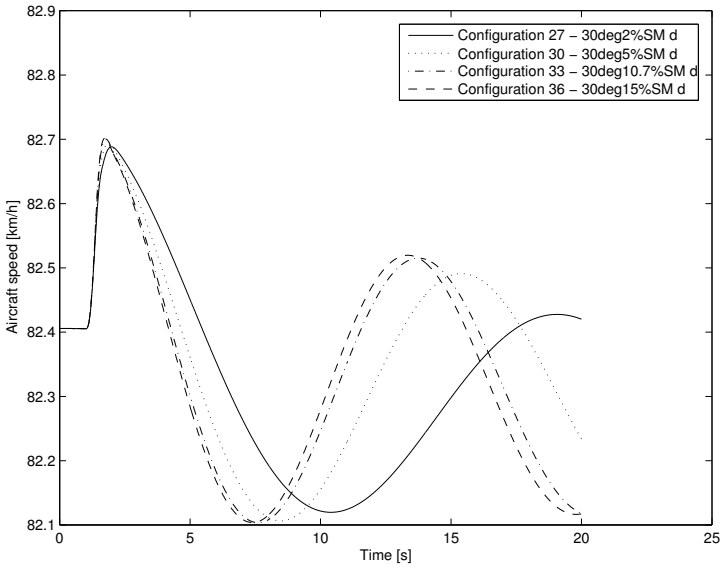

Figure I.35: Gust response for aircraft airspeed for 30° outboard wing sweep at different static margins with the baseline aerodynamic damping.

UNIVERSITEIT VAN PRETORIA
UNIVERSITY OF PRETORIA
YUNIBESITHI YA PRETORIA

I.4 Gust Response Simulations

I.4.1 Configurations 15, 18, 21, 24

Simulation results of all static margin variations at 24° sweep having the baseline aerodynamic damping. (Configurations 15, 18, 21, 24)

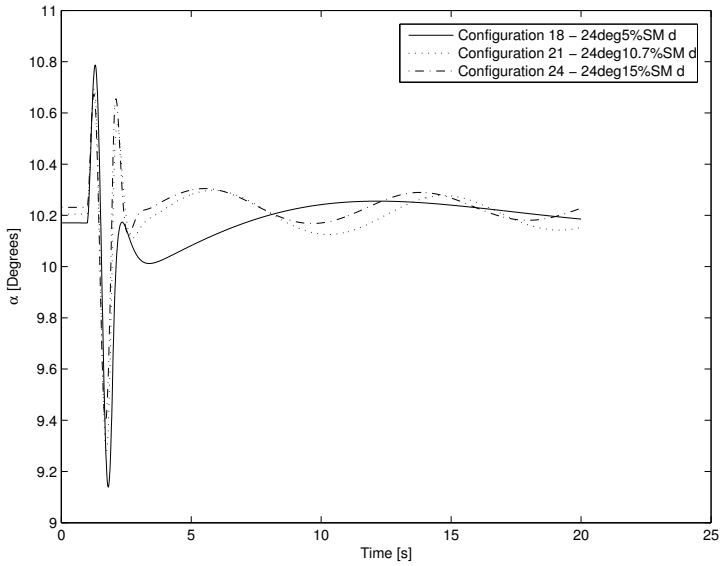

Figure I.36: Gust response for aircraft angle of attack (α) for 24° outboard wing sweep at different static margins with the baseline aerodynamic damping.

UNIVERSITEIT VAN PRETORIA
UNIVERSITY OF PRETORIA
YUNIBESITHI YA PRETORIA

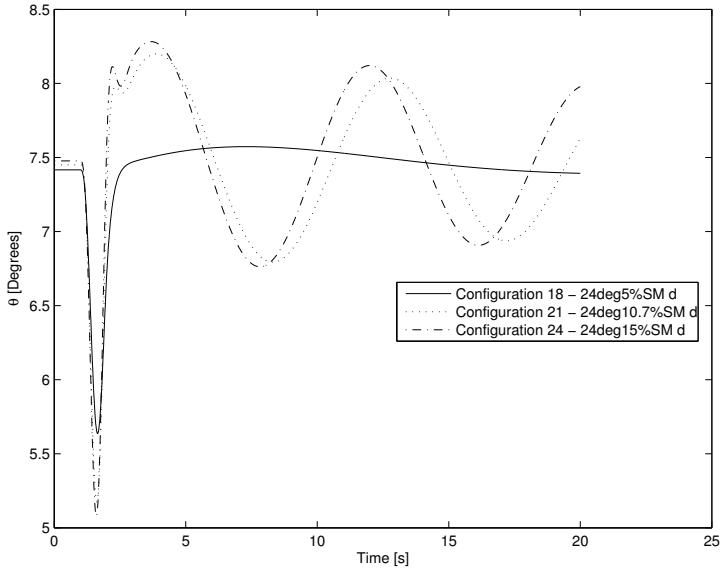

Figure I.37: Gust response for aircraft attitude (θ) for 24° outboard wing sweep at different static margins with the baseline aerodynamic damping.

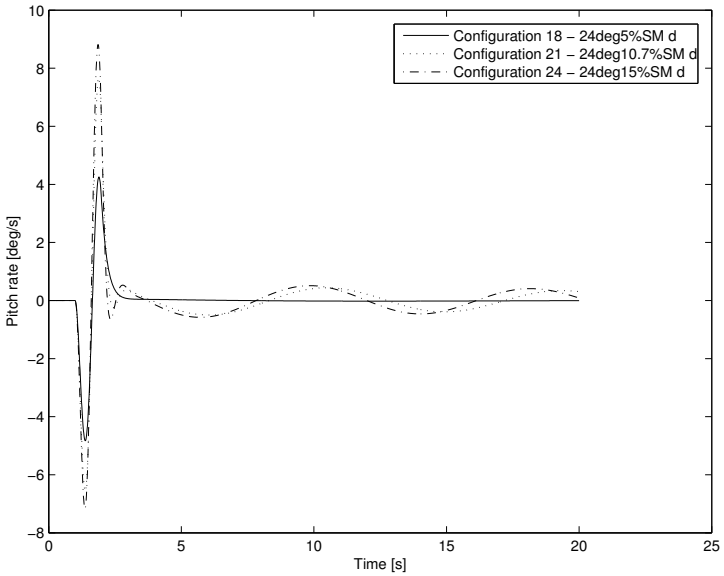

Figure I.38: Gust response for aircraft pitch rate for 24° outboard wing sweep at different static margins with the baseline aerodynamic damping.

UNIVERSITEIT VAN PRETORIA
UNIVERSITY OF PRETORIA
YUNIBESITHI YA PRETORIA

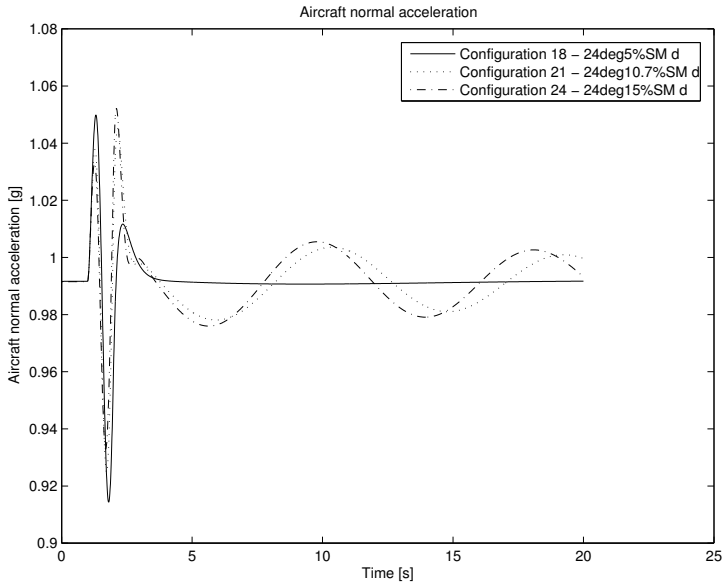

Figure I.39: Gust response for aircraft normal acceleration for 24° outboard wing sweep at different static margins with the baseline aerodynamic damping.

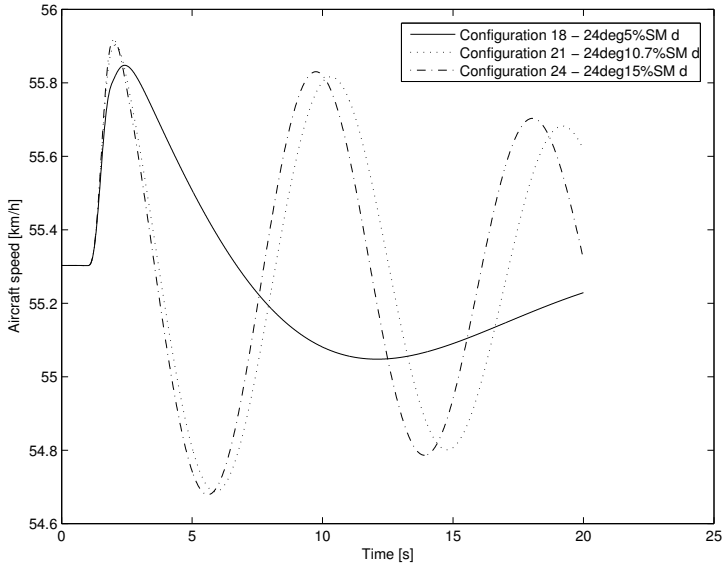

Figure I.40: Gust response for aircraft airspeed for 24° outboard wing sweep at different static margins with the baseline control authority and aerodynamic damping.

UNIVERSITEIT VAN PRETORIA
UNIVERSITY OF PRETORIA
YUNIBESITHI YA PRETORIA

I.4.2 Configurations 39, 42, 45, 48

Simulation results of all static margin variations at 36° sweep having the baseline aerodynamic damping. (Configurations 39, 42, 45, 48)

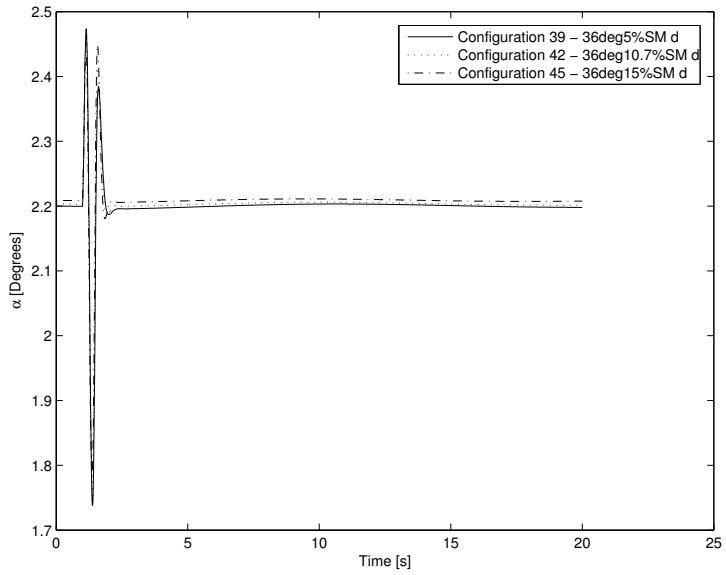

Figure I.41: Gust response for aircraft angle of attack (α) for 36° outboard wing sweep at different static margins with the baseline aerodynamic damping.

UNIVERSITEIT VAN PRETORIA
UNIVERSITY OF PRETORIA
YUNIBESITHI YA PRETORIA

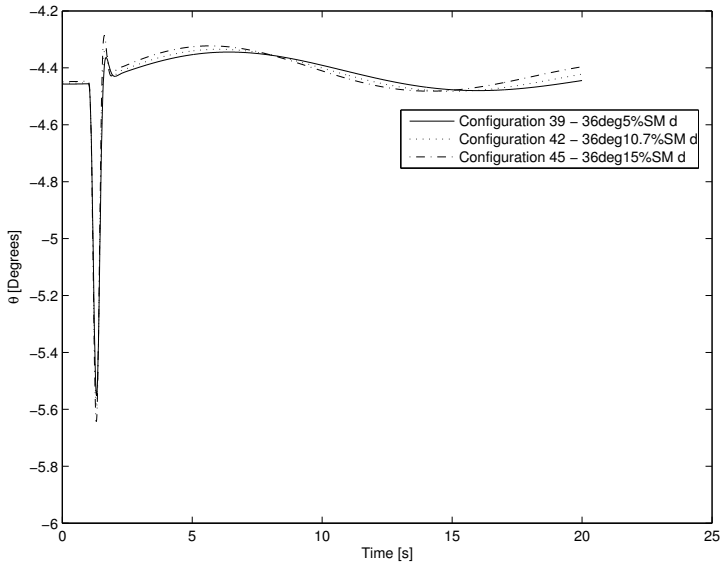

Figure I.42: Gust response for aircraft attitude (θ) for 36° outboard wing sweep at different static margins with the baseline aerodynamic damping.

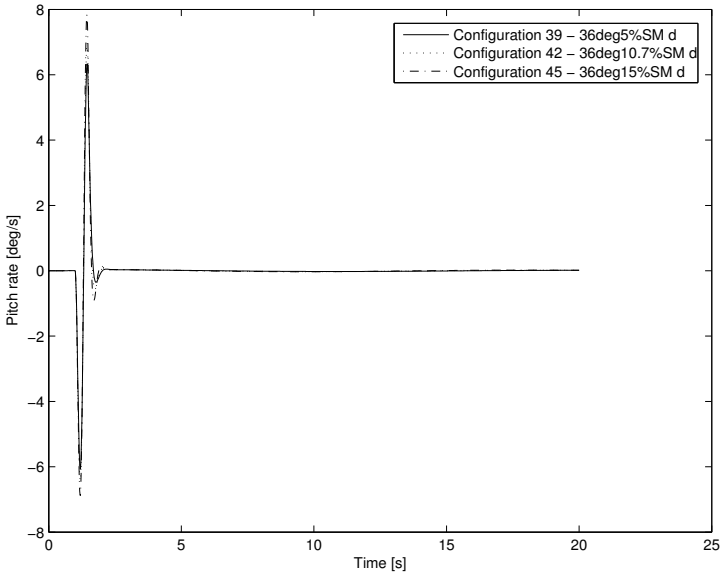

Figure I.43: Gust response for aircraft pitch rate for 36° outboard wing sweep at different static margins with the baseline aerodynamic damping.

UNIVERSITEIT VAN PRETORIA
UNIVERSITY OF PRETORIA
YUNIBESITHI YA PRETORIA

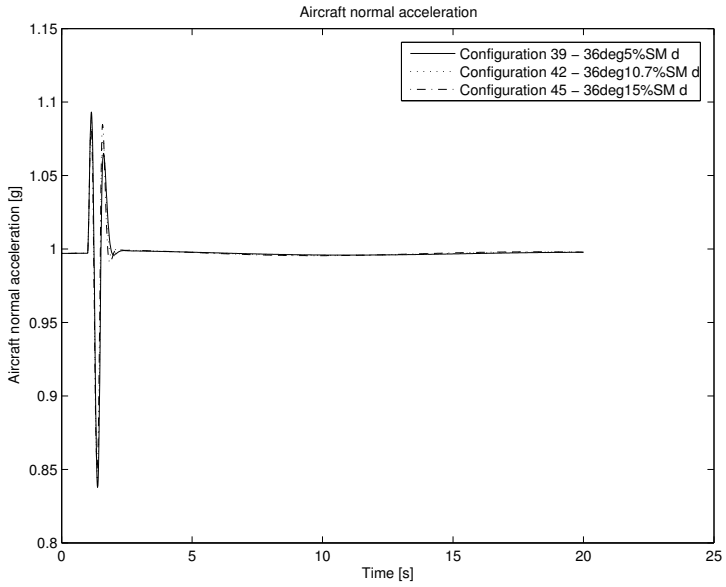

Figure I.44: Gust response for aircraft normal acceleration for 36° outboard wing sweep at different static margins with the baseline aerodynamic damping.

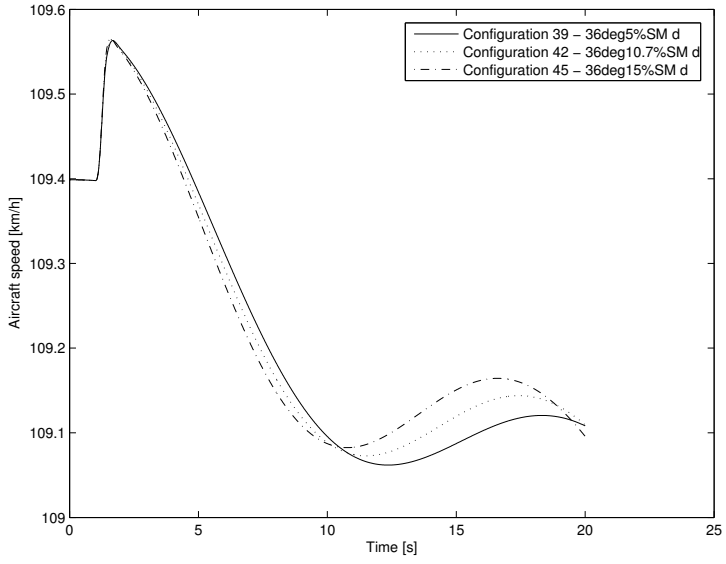

Figure I.45: Gust response for aircraft airspeed for 36° outboard wing sweep at different static margins with the baseline control authority and aerodynamic damping.

UNIVERSITEIT VAN PRETORIA
UNIVERSITY OF PRETORIA
YUNIBESITHI YA PRETORIA

I.4.3 Configurations 31, 32, 33

Simulation results of all damping variations at 30° sweep at a 10.7% (at 30°) static margin configuration. (Configurations 31, 32, 33)

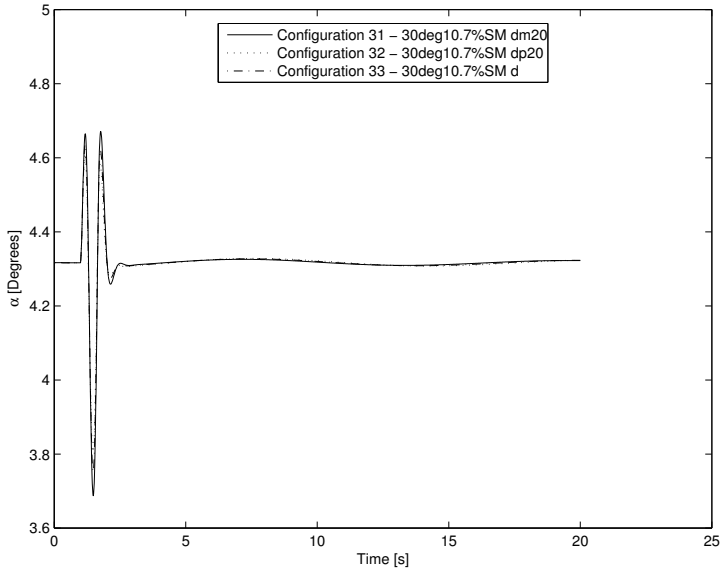

Figure I.46: Gust response for aircraft angle of attack (α) for 30° outboard wing sweep at a 10.7% static margin (at 30° sweep) with different configurations for aerodynamic damping.

UNIVERSITEIT VAN PRETORIA
UNIVERSITY OF PRETORIA
YUNIBESITHI YA PRETORIA

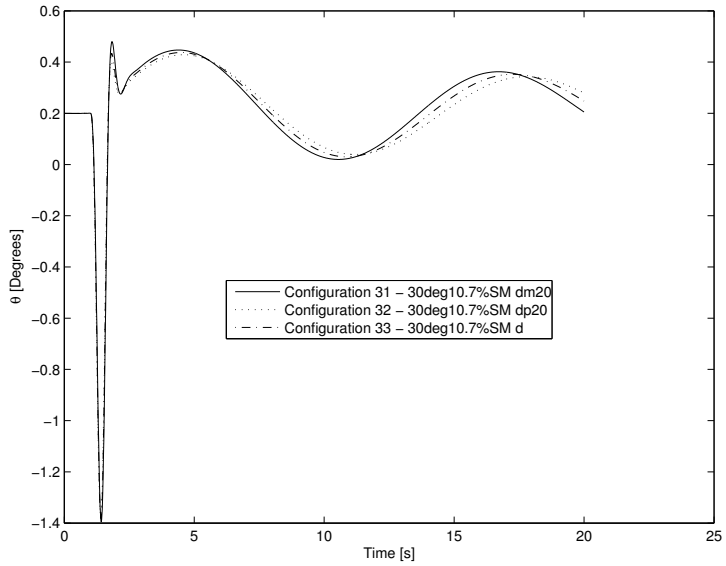

Figure I.47: Gust response for aircraft attitude (θ) for 30° outboard wing sweep at a 10.7% static margin (at 30° sweep) with different configurations for aerodynamic damping.

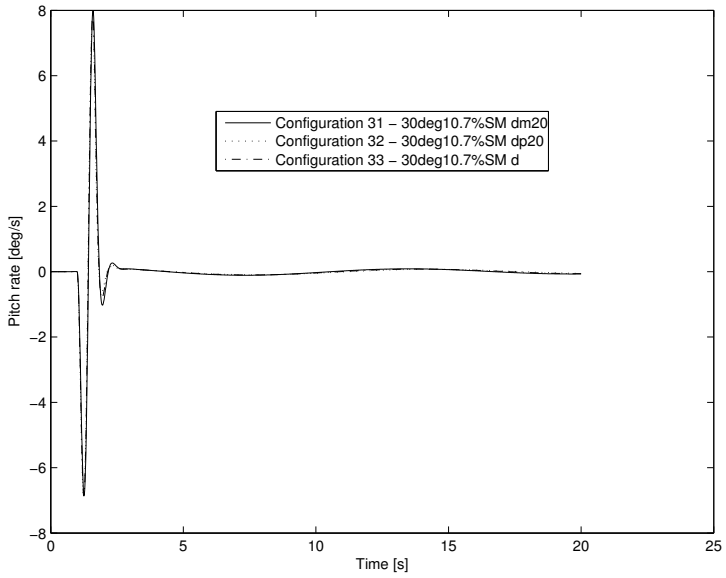

Figure I.48: Gust response for aircraft pitch rate for 30° outboard wing sweep at a 10.7% static margin (at 30° sweep) with different configurations for aerodynamic damping.

UNIVERSITEIT VAN PRETORIA
UNIVERSITY OF PRETORIA
YUNIBESITHI YA PRETORIA

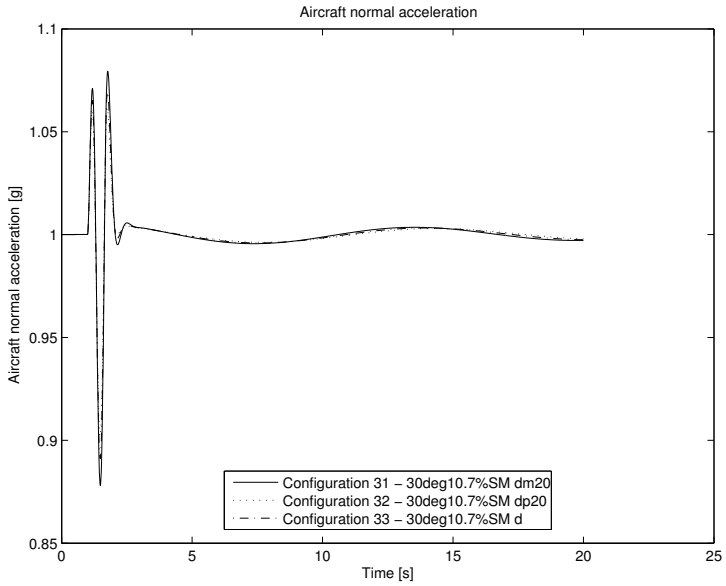

Figure I.49: Gust response for aircraft normal acceleration for 30° outboard wing sweep at a 10.7% static margin (at 30° sweep) with different configurations for aerodynamic damping.

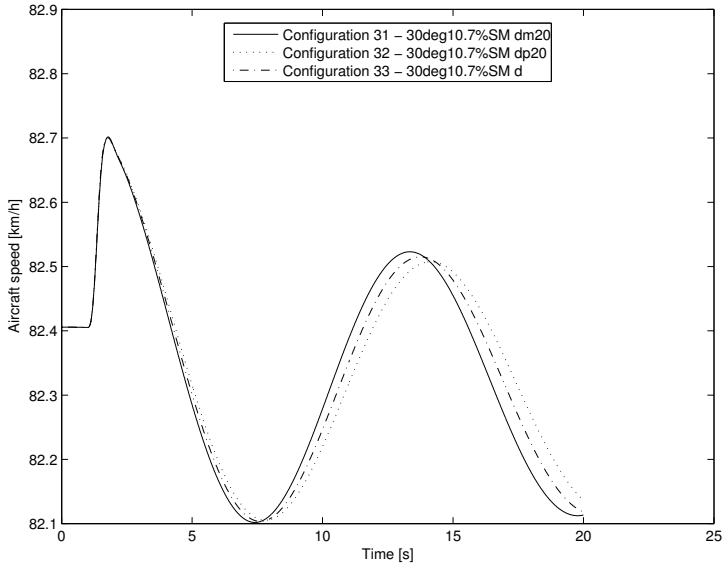

Figure I.50: Gust response for aircraft airspeed for 30° outboard wing sweep at a 10.7% static margin (at 30° sweep) with different configurations for aerodynamic damping.

UNIVERSITEIT VAN PRETORIA
UNIVERSITY OF PRETORIA
YUNIBESITHI YA PRETORIA

I.5 C-star Analysis Results

The additional results of the C-star analysis are presented here.

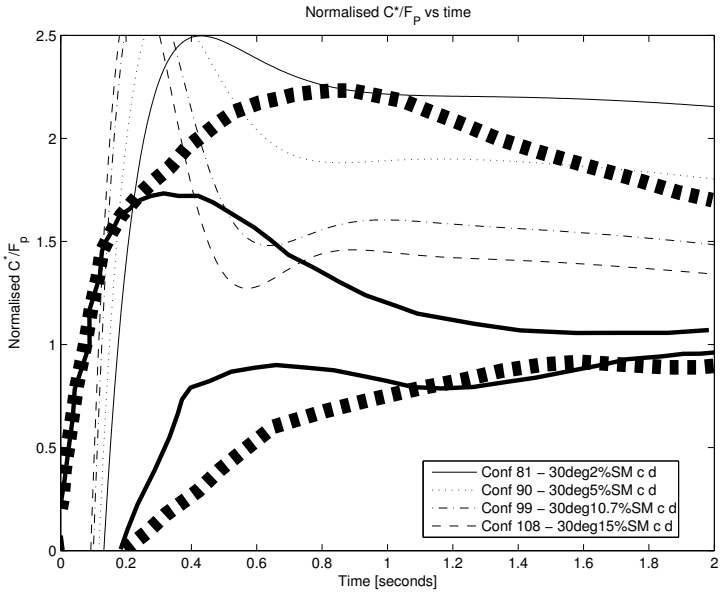

Figure I.51: The C-star analysis for all static margin variations at 30° sweep having the baseline aerodynamic damping and control authority. (Configurations 81, 90, 99, 108).

UNIVERSITEIT VAN PRETORIA
UNIVERSITY OF PRETORIA
YUNIBESITHI YA PRETORIA

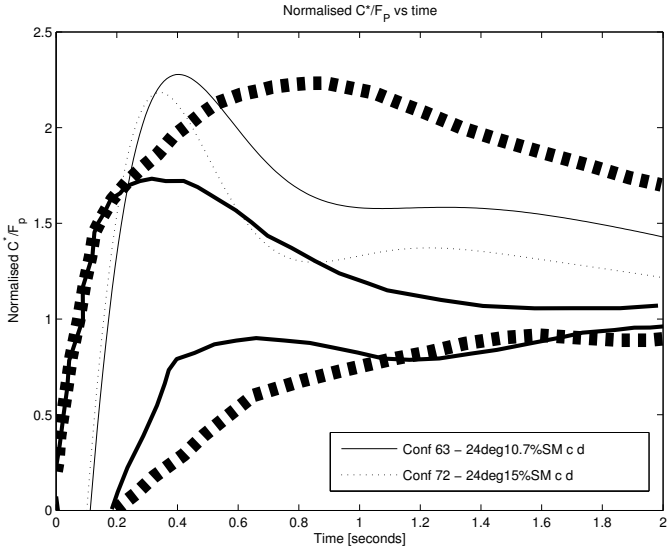

Figure I.52: The C-star analysis for all static margin variations at 24° sweep having the baseline aerodynamic damping and control authority. (Configurations 63, 72).

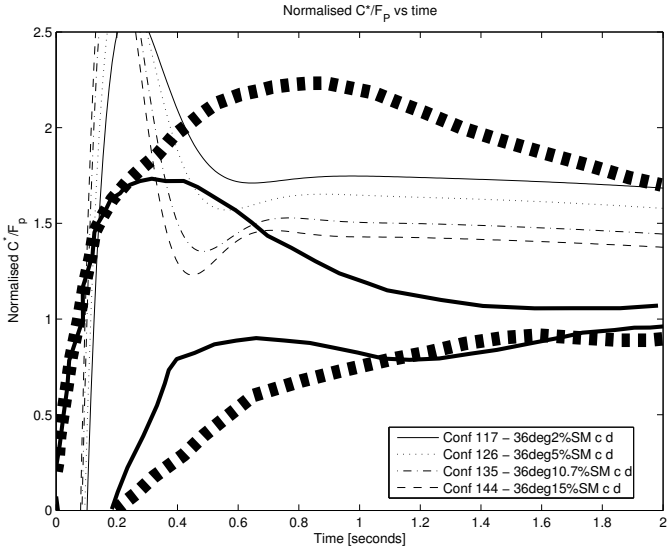

Figure I.53: The C-star analysis for all static margin variations at 36° sweep having the baseline aerodynamic damping and control authority. (Configurations 117, 126, 135, 144)

UNIVERSITEIT VAN PRETORIA
UNIVERSITY OF PRETORIA
YUNIBESITHI YA PRETORIA

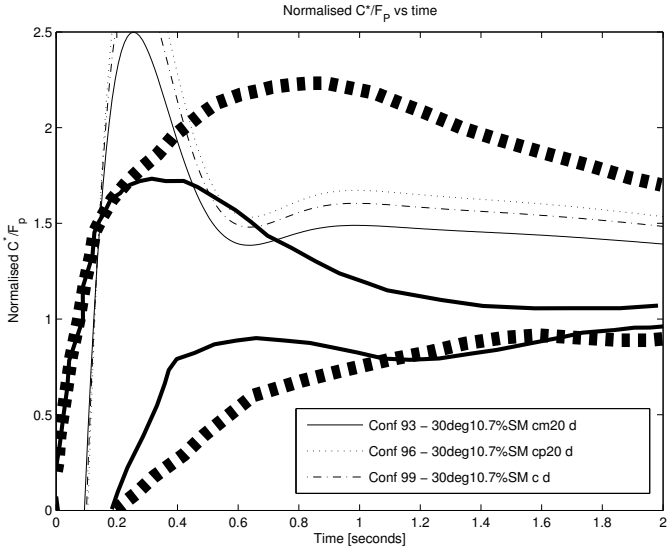

Figure I.54: The C-star analysis for all control authority variations at 30° sweep with the baseline aerodynamic damping at a 10.7% (at 30°) static margin configuration. (Configurations 93, 96, 99)

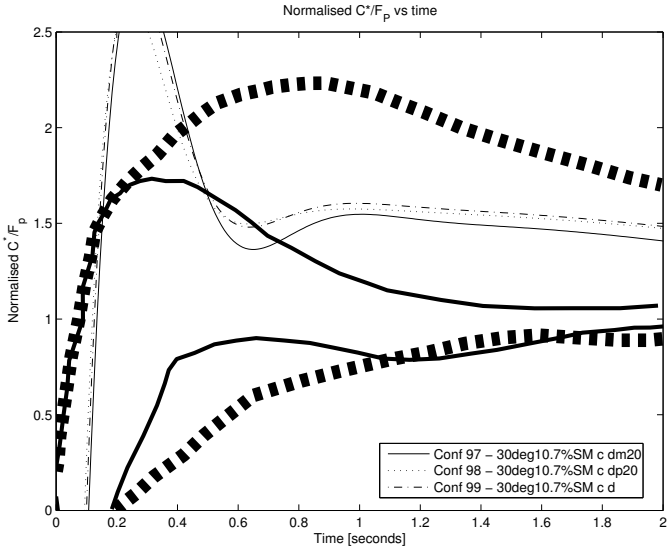

Figure I.55: The C-star analysis for all damping variations at 30° sweep with the baseline control authority at a 10.7% (at 30°) static margin configuration. (Configurations 97, 98, 99)

Appendix J

Frequency Domain Analysis Results

J.1 Thumbprint Criterion Analysis

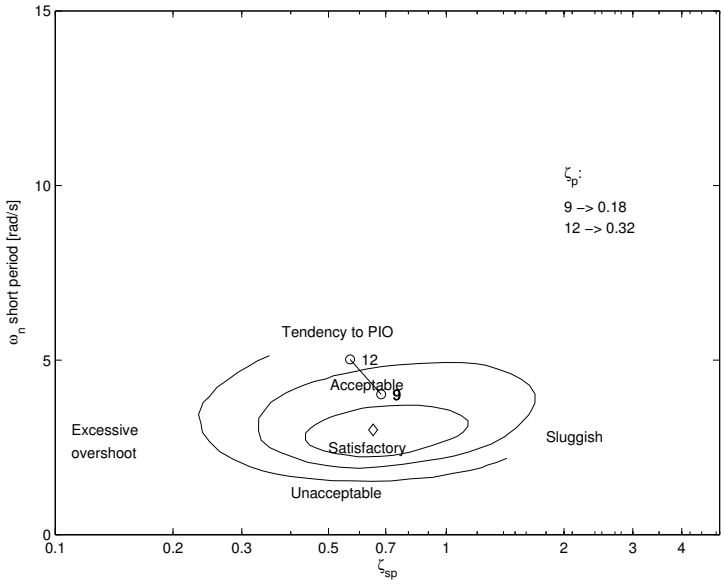

Figure J.1: Thumbprint analysis for 20° outboard wing sweep, at various static margin cases, with the baseline aerodynamic damping.

UNIVERSITEIT VAN PRETORIA
UNIVERSITY OF PRETORIA
YUNIBESITHI YA PRETORIA

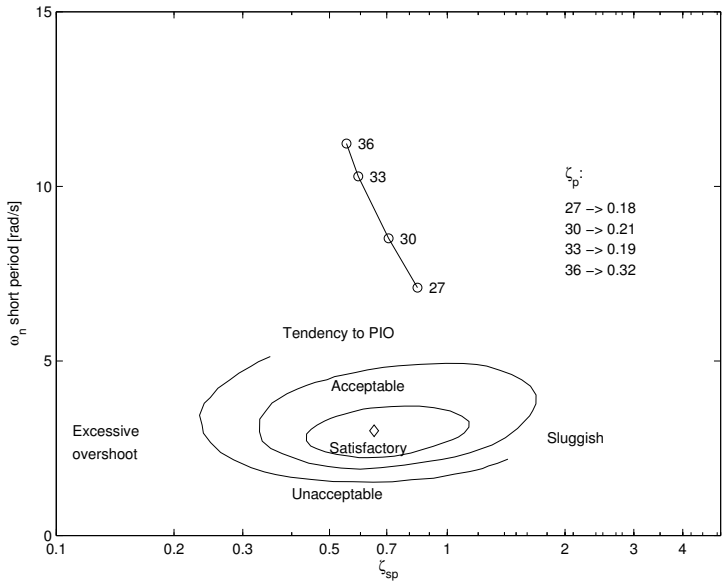

Figure J.2: Thumbprint analysis for 30° outboard wing sweep, at various static margin cases, with the baseline aerodynamic damping.

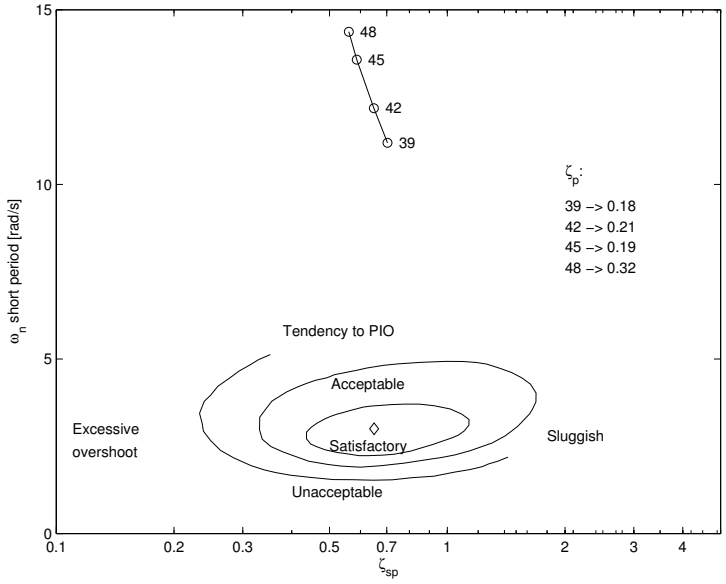

Figure J.3: Thumbprint analysis for 36° outboard wing sweep, at various static margin cases, with the baseline aerodynamic damping.

UNIVERSITEIT VAN PRETORIA
UNIVERSITY OF PRETORIA
YUNIBESITHI YA PRETORIA

J.2 Military Flying Qualities Analysis

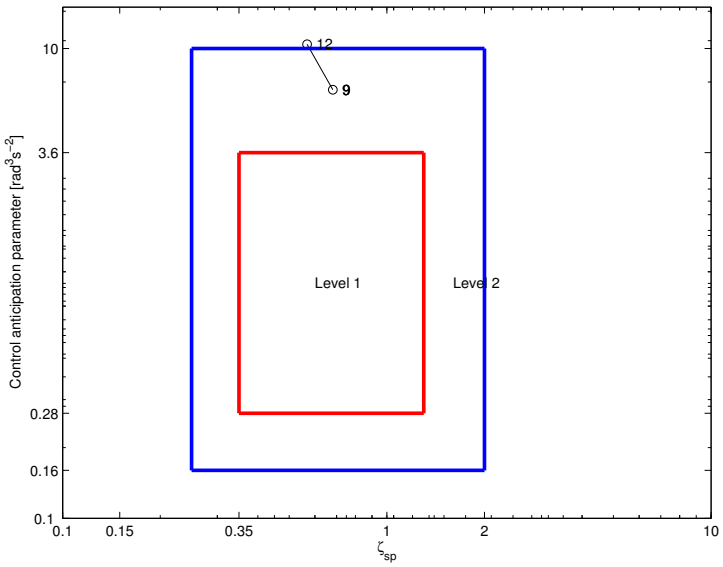

Figure J.4: *CAP* for 20° outboard wing sweep, at various static margin cases, with the baseline aerodynamic damping.

UNIVERSITEIT VAN PRETORIA
UNIVERSITY OF PRETORIA
YUNIBESITHI YA PRETORIA

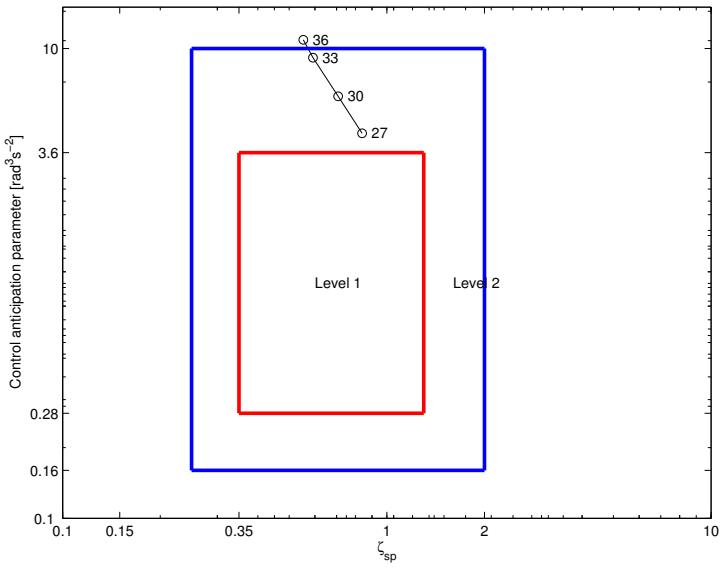

Figure J.5: *CAP* for 30° outboard wing sweep, at various static margin cases, with the baseline aerodynamic damping.

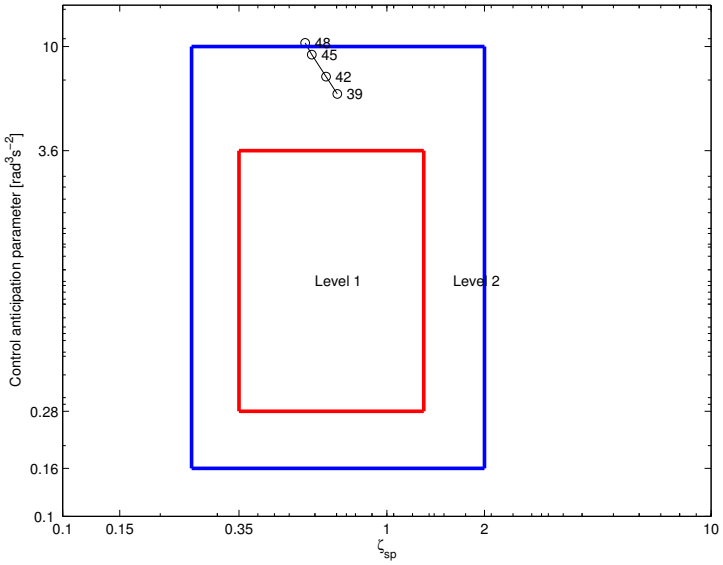

Figure J.6: *CAP* for 36° outboard wing sweep, at various static margin cases, with the baseline aerodynamic damping.

UNIVERSITEIT VAN PRETORIA
UNIVERSITY OF PRETORIA
YUNIBESITHI YA PRETORIA

J.3 Shomber-Gertsen Analysis

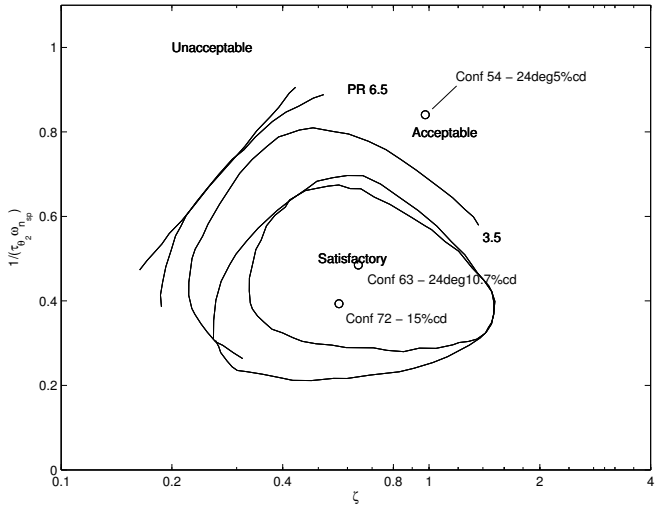

Figure J.7: Group two analysis results for $n_\alpha < 15$ g/rad.

UNIVERSITEIT VAN PRETORIA
UNIVERSITY OF PRETORIA
YUNIBESITHI YA PRETORIA

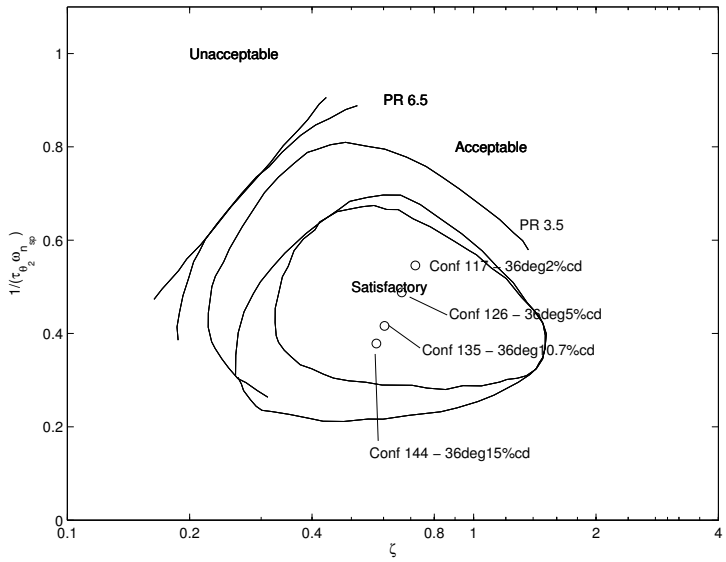

Figure J.8: Group three analysis results for $n_\alpha < 15$ g/rad.

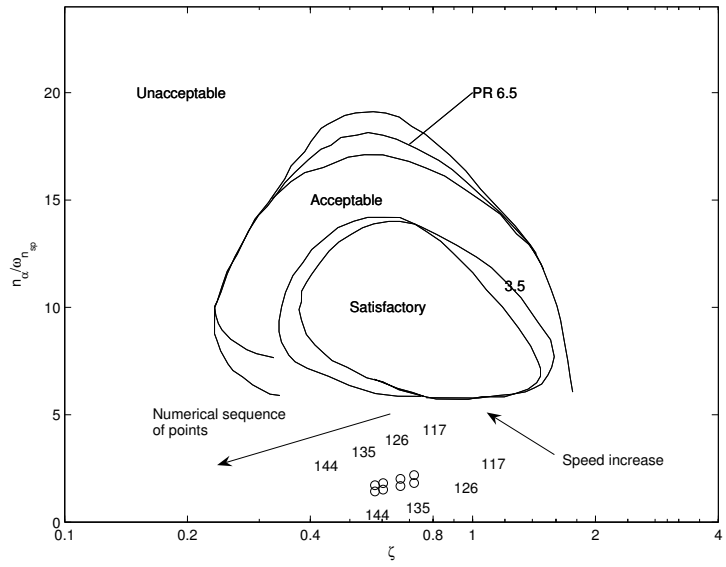

Figure J.9: Group three analysis results for $n_\alpha \geq 15$ g/rad.

UNIVERSITEIT VAN PRETORIA
UNIVERSITY OF PRETORIA
YUNIBESITHI YA PRETORIA

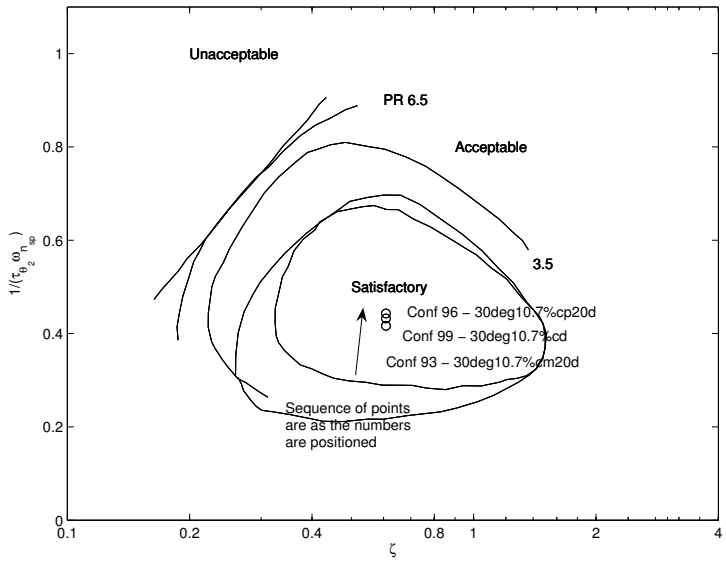

Figure J.10: Group four analysis results for $n_\alpha < 15$ g/rad.

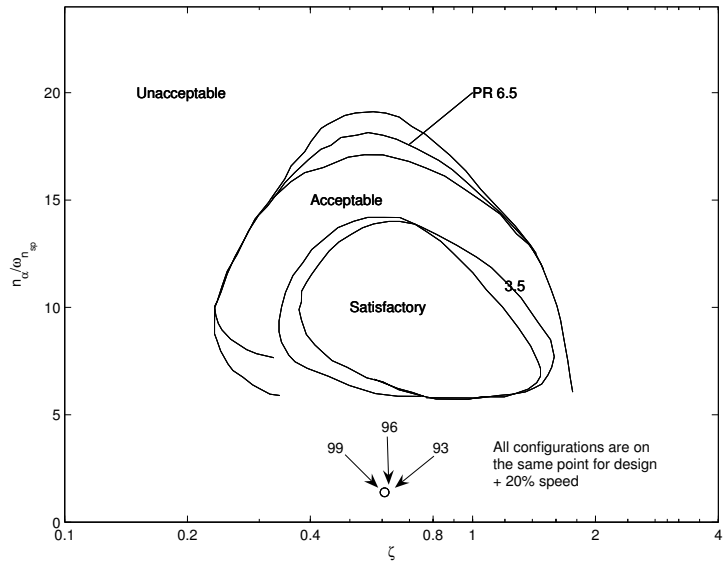

Figure J.11: Group four analysis results for $n_\alpha \geq 15$ g/rad.

UNIVERSITEIT VAN PRETORIA
UNIVERSITY OF PRETORIA
YUNIBESITHI YA PRETORIA

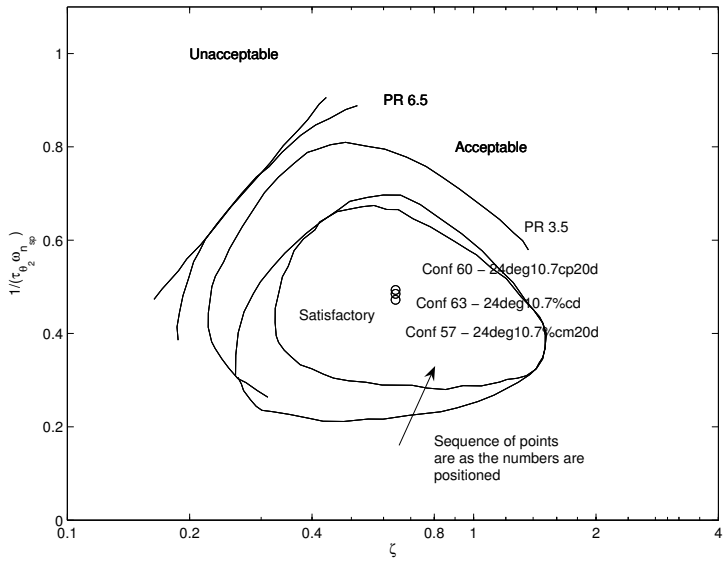

Figure J.12: Group five analysis results for $n_\alpha < 15$ g/rad.

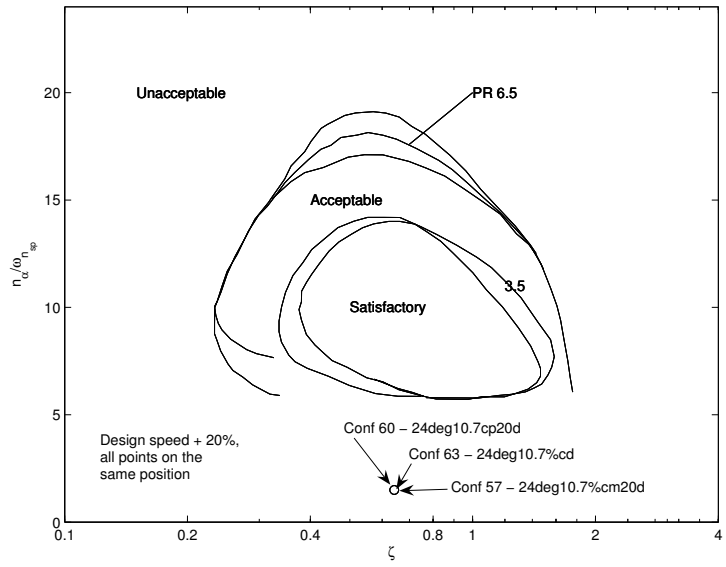

Figure J.13: Group five analysis results for $n_\alpha \geq 15$ g/rad.

UNIVERSITEIT VAN PRETORIA
UNIVERSITY OF PRETORIA
YUNIBESITHI YA PRETORIA

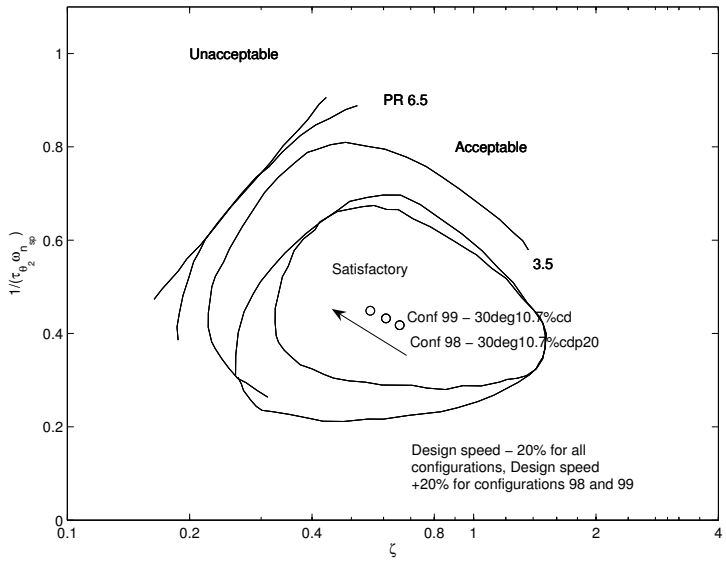

Figure J.14: Group six analysis results for $n_\alpha < 15$ g/rad.

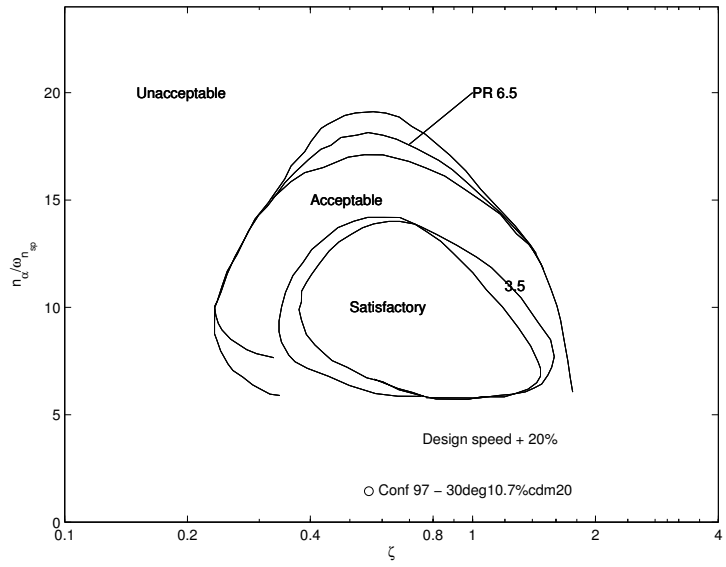

Figure J.15: Group six analysis results for $n_\alpha \geq 15$ g/rad.

Appendix K

Neal-Smith Example

The Neal-Smith method will now be presented by means of an example. A sample Neal-Smith analysis of configuration 99 (30° sweep, 10.7% static margin and the baseline control authority and aerodynamic damping) of the gull-wing configuration will be presented.

The first step of the Neal-Smith analysis of configuration 99 was to set up the transfer function of the aircraft configuration using Equation 3.9 and the aerodynamic coefficients for this configuration that was presented in Chapter 4:

$$\frac{\theta}{F_s} = \frac{K_\theta(\tau_{\theta_2}s + 1)}{s(\frac{s^2}{\omega_{sp}^2} + \frac{2\zeta_{sp}}{\omega_{n_{sp}}}s + 1)} \tag{K.1}$$

The open loop Bode amplitude and phase characteristics for the aircraft transfer function together with a pilot time delay and a gain of 1 was consequently calculated for a frequency range from 0 to 10 rad/s. The results were plotted onto a Nichols chart and translated vertically (which implies merely a open loop gain adjustment) until the 3.5 rad/s point fell on the 90° closed loop phase angle or alternatively until the hump of the graph fell onto the 3 dB droop boundary. The result of this plot is shown in Figure K.1.

After the gain adjusted uncompensated curve is plotted on the Nichols chart it is necessary to choose whether to use lead or lag in order to achieve the performance standards (3.5 rad/s bandwidth and the maximum of 3 dB droop). This process mimics the way a pilot would adapt to an aircraft in

UNIVERSITEIT VAN PRETORIA
UNIVERSITY OF PRETORIA
YUNIBESITHI YA PRETORIA

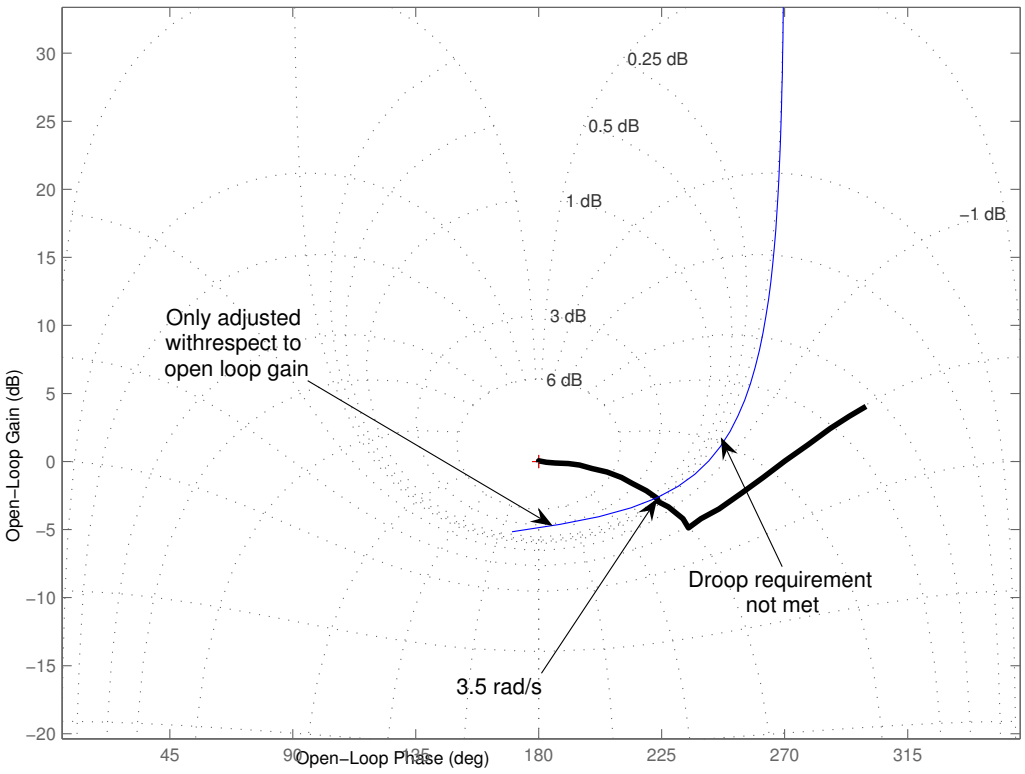

Figure K.1: Nichols chart for aircraft configuration 99 with only gain adjustment in order to achieve the performance standards.

order to perform flying tasks with the aircraft. Figure K.2 shows examples of configurations that require lead or lag compensation. Curve A is an example of an aircraft that requires lag compensation. The droop requirement is satisfied for this curve because the hump of the curve forms a tangent with the -3 dB line on the Nichols chart, but the 3.5 rad/s frequency does not lie on the -90° (or the 270°) phase line. Even though the bandwidth of this configuration might be higher than 3.5 rad/s, the closed loop resonance of the aircraft configuration that Curve A represents, will be high. This means that the aircraft will suffer from *PIO*. An aircraft will have reduced closed loop resonance (and accompanying good handling characteristics) only when both performance criteria (bandwidth and droop) are satisfied. Curve B is an example of an aircraft that requires lead compensation. The 3.5 rad/s frequency lies on the -90° phase line, but the hump of the curve does not

UNIVERSITEIT VAN PRETORIA
UNIVERSITY OF PRETORIA
YUNIBESITHI YA PRETORIA

lie on the -3 dB boundary. Once again, even though the droop is less than 3 dB, the closed loop resonance is higher than what it could be with the lead compensation.

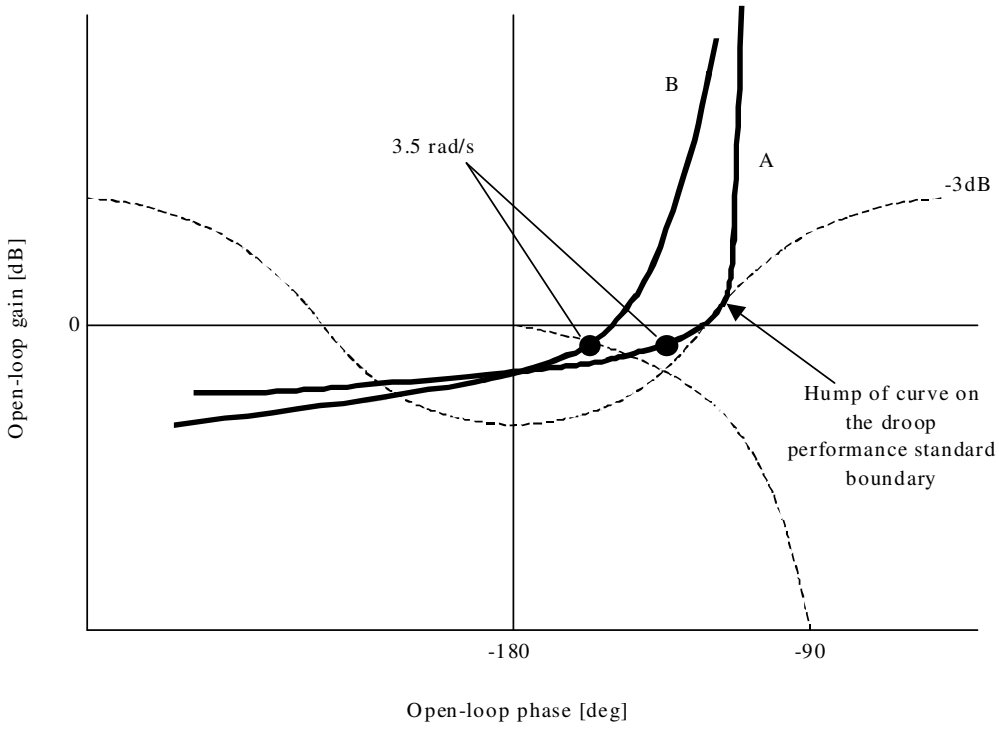

Figure K.2: Nichols chart illustrating the difference between a system that requires lead and lag compensation.

Neal & Smith (1970) defines 'rules' for determining the optimum lead or lag. The reference mentions that these rules might not represent the absolute optimum (such as would be achieved by a optimisation routine), but that the lead/lag guidelines provide very close to optimum compensation, as well as a repeatable process with which to determine compensation values. For purposes of comparison with the Neal-Smith document the same rules for determining lead and lag were employed in the gull-wing configuration analysis.

The lead/lag 'rules' state that if lead compensation is required, the lag time constant (τ_{p_2}) must be set to zero. The lead time constant is then varied

UNIVERSITEIT VAN PRETORIA
UNIVERSITY OF PRETORIA
YUNIBESITHI YA PRETORIA

in an iterative process until the performance criteria are met.

If lag compensation is required, the optimum lead and lag time constants are chosen so that the lead and lag frequencies ($1/\tau_{p_1}$ and $1/\tau_{p_2}$) are logarithmically centred around the minimum bandwidth frequency (BW_{MIN}). This implies that the ratio between the lag and lead time constants or $\frac{\tau_{p_2}}{\tau_{p_1}}$ is chosen in an iterative process.

Once the ratio is chosen, the lead time constant is calculated using Equation K.2. The lag time constant may then be found using the ratio and the lead time constant value.

$$\tau_{p_1} = \frac{1}{x^{\frac{1}{2}} BW_{MIN}} \tag{K.2}$$

If Figure K.1 is studied, it is clear that lead compensation is required, because the droop requirement is not met. τ_{p_1} was consequently varied and the Nichols chart was plotted for the different values until all the requirements of the performance criteria were met. The result of the process is presented in Figure K.3. This graph represents a transfer function that satisfies the 3.5 rad/s bandwidth as well as the minimum droop requirement of 3 dB.

The Bode plot of the airframe that is compensated by the optimised compensation network can now be plotted and this is presented in Figure K.5. The resonant peak of the closed loop system (or peak of the $\frac{\theta}{\theta_c}$ magnitude Bode plot) may be read off from this graph. The phase angle of the pilot compensation at the bandwidth frequency of 3.5 rad/s may now be read off a Bode plot of the compensation network alone (see Figure K.4), or by using Figure 3.10. The resonant peak of the compensated airframe and the phase angle of pilot compensation are then used as y and x co-ordinates respectively and plotted on the pilot opinion map presented in Figure 3.6. A step response of the optimised closed loop transfer function is shown in Figure K.6.

UNIVERSITEIT VAN PRETORIA
UNIVERSITY OF PRETORIA
YUNIBESITHI YA PRETORIA

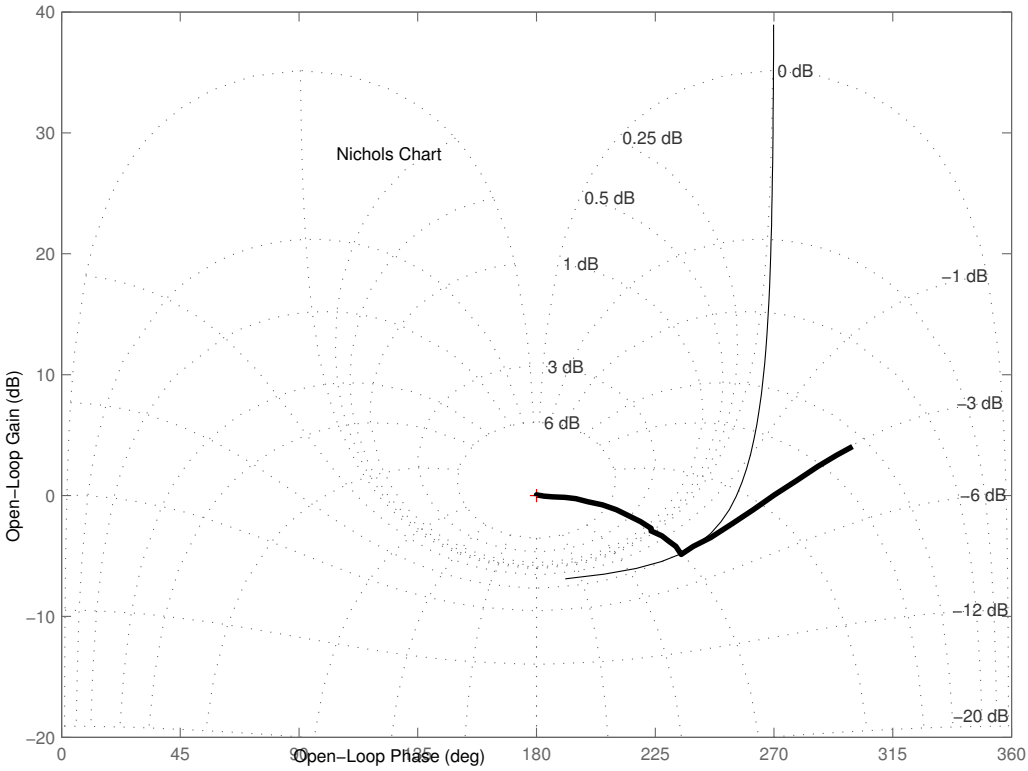

Figure K.3: Nichols chart for aircraft configuration 99 with lead, lag and gain adjustment in order to achieve the performance standards.

UNIVERSITEIT VAN PRETORIA
UNIVERSITY OF PRETORIA
YUNIBESITHI YA PRETORIA

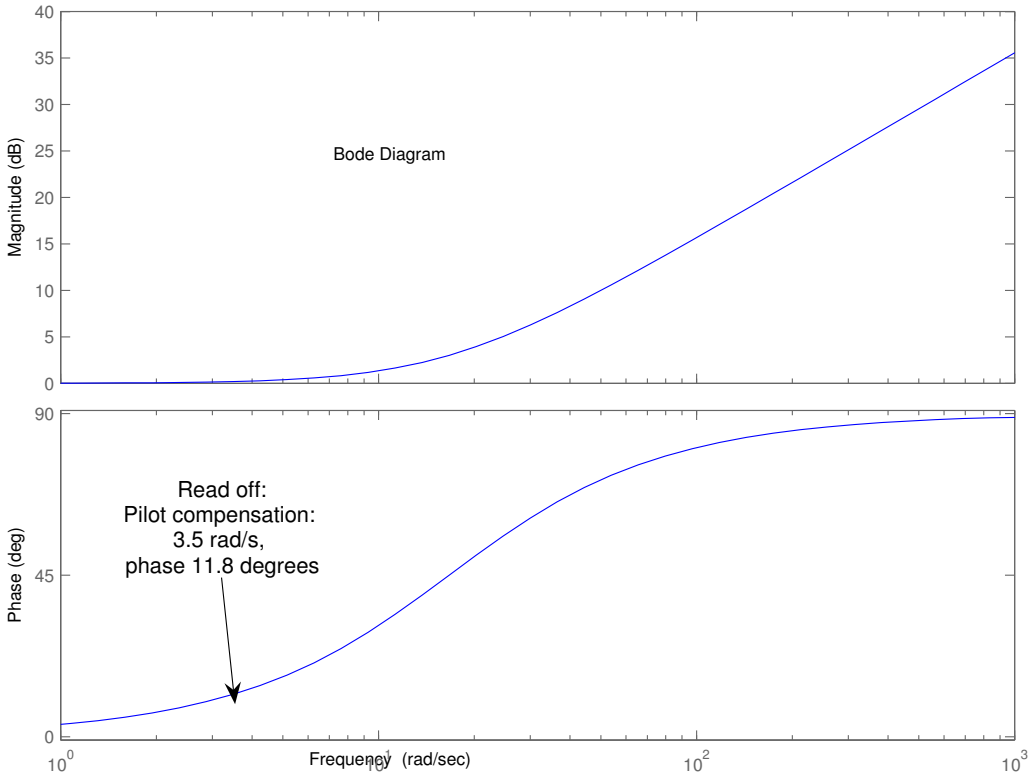

Figure K.4: Bode plot of the pilot compensation network. The phase angle at 3.5 rad/s is indicated by an arrow.

UNIVERSITEIT VAN PRETORIA
UNIVERSITY OF PRETORIA
YUNIBESITHI YA PRETORIA

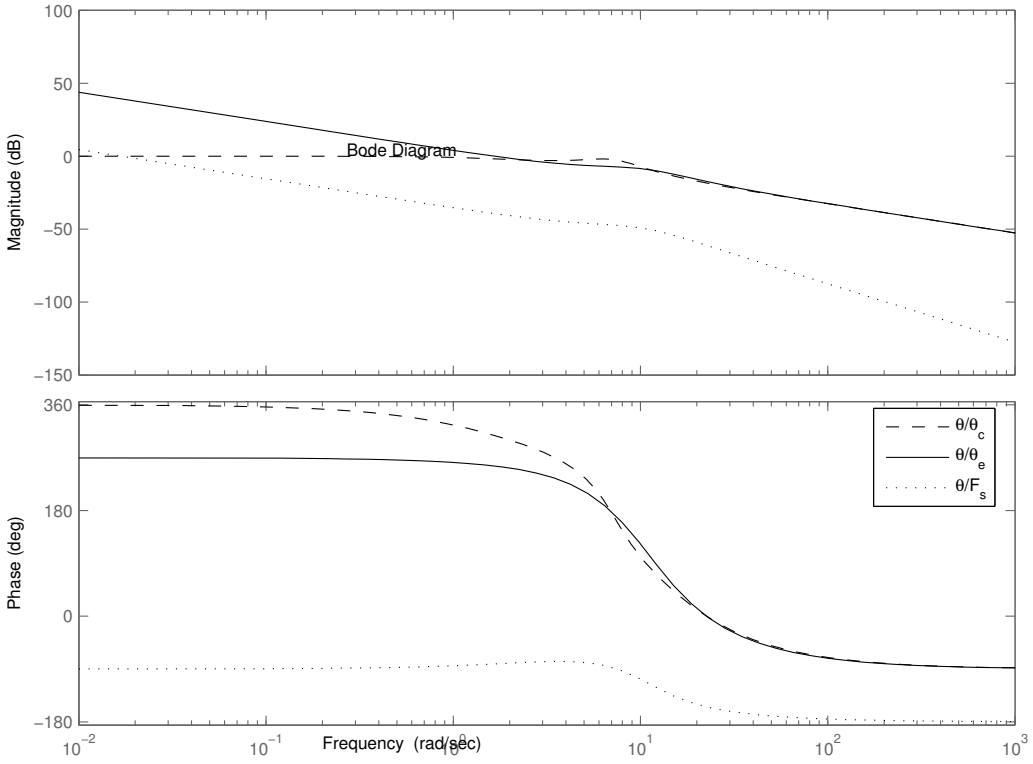

Figure K.5: Bode plots for aircraft configuration 99 showing the Bode characteristics of the airframe only, the open loop as well as the closed loop pilot compensated aircraft transfer function.

UNIVERSITEIT VAN PRETORIA
UNIVERSITY OF PRETORIA
YUNIBESITHI YA PRETORIA

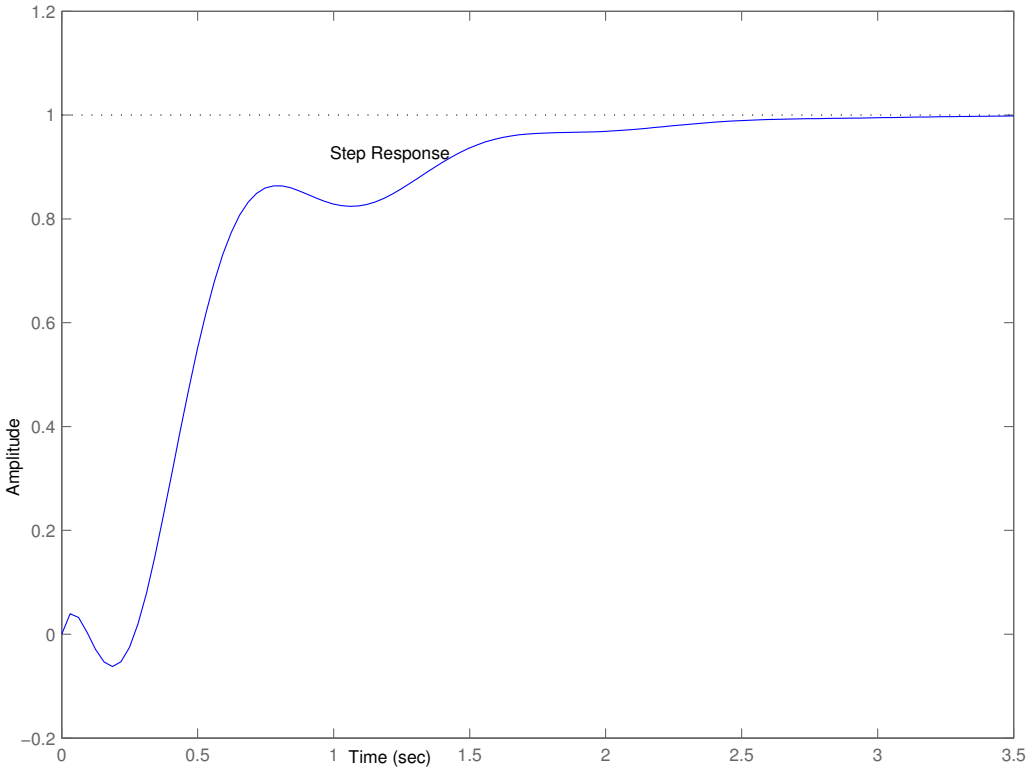

Figure K.6: Step response for the closed loop pilot compensated aircraft configuration 99.

UNIVERSITEIT VAN PRETORIA
UNIVERSITY OF PRETORIA
YUNIBESITHI YA PRETORIA

Appendix L

Longitudinal Transfer Functions

The equations presented here were obtained from Appendix IV of Neal & Smith (1970). These equations represent the linearised version of Equation 4.1. The linearisation is performed at an arbitrary trim point. The equations are included for purposes of completeness and serve to support the Neal-Smith analysis presented in Section 7.4. The Neal-Smith analysis uses the transfer functions presented in this section.

Several simplified longitudinal transfer functions are presented in the following paragraphs. The following equations of motion are used to represent the airplane pitch dynamics. They assume constant speed and neglect incremental effects of gravity.

$$\begin{aligned} \ddot{\theta} &= M_q\dot{\theta} + M_{\dot{\alpha}}\dot{\alpha} + M_\alpha\alpha + M_{\delta_e}\delta_e \\ \dot{\alpha} &= \dot{\theta} - L_\alpha\alpha - L_{\delta_e}\delta_e \\ n &= \frac{V_T}{g}(\dot{\theta} - \dot{\alpha}) \end{aligned} \tag{L.1}$$

The equations imply that the reference axes are stability axes and that the wings are always level so that $\dot{\theta} = q$ and $\theta(s) = \frac{1}{s}\dot{\theta}(s)$. Small disturbances

UNIVERSITEIT VAN PRETORIA
UNIVERSITY OF PRETORIA
YUNIBESITHI YA PRETORIA

are assumed, so that the variables θ, α, n and δ_e differ only by small amounts from their respective trim conditions.

The following transfer functions in Laplace notation arise from the above equations:

$$\begin{aligned}
\frac{q}{\delta_e} &= \frac{(M_{\delta_e} - L_{\delta_e}M_{\dot{\alpha}})s + (M_{\delta_e}L_\alpha - M_\alpha L_{\delta_e})}{s^2 + (L_\alpha - M_q - M_{\dot{\alpha}})s - (M_\alpha + M_q L_\alpha)} \\
\frac{\alpha}{\delta_e} &= \frac{-L_{\delta_e}s + (M_{\delta_e} + M_q L_{\delta_e})}{s^2 + (L_\alpha - M_q - M_{\dot{\alpha}})s - (M_\alpha + M_q L_\alpha)} \\
\frac{n}{\delta_e} &= \left(\frac{V_T}{g}\right)\frac{L_{\delta_e}s^2 + (-L_{\delta_e}M_q - L_{\delta_e}M_{\dot{\alpha}})s + (M_{\delta_e}L_\alpha - M_\alpha L_{\delta_e})}{s^2 + (L_\alpha - M_q - M_{\dot{\alpha}})s - (M_\alpha + M_q L_\alpha)}
\end{aligned} \tag{L.2}$$

Assuming that the product of small terms is negligible $L_{\delta_e}M_q \approx L_{\delta_e}M_{\dot{\alpha}} \approx 0$:

$$\begin{aligned}
\frac{q}{\delta_e} &= \frac{M_{\delta_e}s + (M_{\delta_e}L_\alpha - M_\alpha L_{\delta_e})}{s^2 + (L_\alpha - M_q - M_{\dot{\alpha}})s - (M_\alpha + M_q L_\alpha)} \\
\frac{\alpha}{\delta_e} &= \frac{-L_{\delta_e}s + M_{\delta_e}}{s^2 + (L_\alpha - M_q - M_{\dot{\alpha}})s - (M_\alpha + M_q L_\alpha)} \\
\frac{n}{\delta_e} &= \left(\frac{V_T}{g}\right)\frac{L_{\delta_e}s^2 + (M_{\delta_e}L_\alpha - M_\alpha L_{\delta_e})}{s^2 + (L_\alpha - M_q - M_{\dot{\alpha}})s - (M_\alpha + M_q + L_\alpha)}
\end{aligned} \tag{L.3}$$

The short-period natural frequency and damping ratio can be expressed as:

$$\begin{aligned}
\omega_{n_{sp}}^2 &= -M_\alpha - M_q L_\alpha \\
2\zeta_{sp}\omega_{n_{sp}} &= L_\alpha - M_q - M_{\dot{\alpha}} \\
\zeta_{sp} &= \frac{L_\alpha - M_q - M_{\dot{\alpha}}}{2\sqrt{-M_\alpha - M_q L_\alpha}}
\end{aligned} \tag{L.4}$$

and:

UNIVERSITEIT VAN PRETORIA
UNIVERSITY OF PRETORIA
YUNIBESITHI YA PRETORIA

$$\frac{1}{\tau_{\theta_2}} = \frac{M_{\delta_e} L_\alpha - M_\alpha L_{\delta_e}}{M_{\delta_e}} \tag{L.5}$$

Making these substitutions and rearranging,

$$\begin{aligned}
\frac{q}{\delta_e} &= \frac{M_{\delta_e}}{\omega_{n_{sp}}^2} \frac{1}{\tau_{\theta_2}} \frac{(\tau_{\theta_2} s + 1)}{\frac{s^2}{\omega_{n_{sp}}^2} + \frac{2\zeta_{sp}}{\omega_{n_{sp}}} s + 1} \\
\frac{\alpha}{\delta_e} &= \frac{M_{\delta_e}}{\omega_{n_{sp}}^2} \frac{(-\frac{L_{\delta_e}}{M_{\delta_e}} s + 1)}{\frac{s^2}{\omega_{n_{sp}}^2} + \frac{2\zeta_{sp}}{\omega_{n_{sp}}} s + 1} \\
\frac{n}{\delta_e} &= \frac{M_{\delta_e}}{\omega_{n_{sp}}^2} \left(\frac{V_T}{g} \frac{1}{\tau_{\theta_2}}\right) \frac{\tau_{\theta_2} \frac{L_{\delta_e}}{M_{\delta_e}} s^2 + 1}{\frac{s^2}{\omega_{n_{sp}}^2} + \frac{2\zeta_{sp}}{\omega_{n_{sp}}} s + 1}
\end{aligned} \tag{L.6}$$

For most conventional airplanes, the numerator time constants in the $\frac{\alpha}{\delta_e}$ and $\frac{n}{\delta_e}$ transfer functions are negligible. However, for airplanes having a tail length which is quite short, these numerator terms can be important.

The following relationships are now derived for use in the Neal-Smith handling characteristics analysis:

1. n/α:
   For a step input in elevon/elevator deflection,

$$\begin{aligned}
\left(\frac{n}{\delta_e}\right)_{SS} &= \left(\frac{n}{\delta_e}\right)|_{s\to 0} = \frac{M_{\delta_e}}{\omega_{n_{sp}}^2} \left(\frac{V_T}{g} \frac{1}{\tau_{\theta_2}}\right) \\
\left(\frac{\alpha}{\delta_e}\right)_{SS} &= \left(\frac{\alpha}{\delta_e}\right)|_{s\to 0} = \frac{M_{\delta_e}}{\omega_{n_{sp}}^2}
\end{aligned}$$

   therefore,

$$\left(\frac{n}{\alpha}\right)_{SS} = \frac{(n/\delta_e)_{SS}}{(\alpha/\delta_e)_{SS}} = \frac{V_T}{g} \frac{1}{\tau_{\theta_2}}$$

UNIVERSITEIT VAN PRETORIA
UNIVERSITY OF PRETORIA
YUNIBESITHI YA PRETORIA

2. F_s/n:

$$\left(\frac{n}{F_s}\right)_{SS} = \left(\frac{n}{\delta_e}\right)_{SS}\left(\frac{\delta_e}{F_s}\right)_{SS}$$

and

$$M_{F_s} = M_{\delta_e}\left(\frac{\delta_e}{F_s}\right)_{SS}$$

therefore,

$$\left(\frac{F_s}{n}\right)_{SS} = \left(\frac{n}{F_s}\right)_{SS}^{-1} = \frac{\omega_{n_{sp}}^2}{M_{F_s}(n/\alpha)_{SS}}$$

3. θ/F_s transfer function (no control system dynamics):

$$\frac{\theta}{F_s} = \frac{\theta}{\delta_e}\left(\frac{\delta_e}{F_s}\right)_{SS} = \frac{M_{F_s}}{\omega_{n_{sp}}^2}\left(\frac{1}{\tau_{\theta_2}}\right)\frac{\tau_{\theta_2}s+1}{s\left(\frac{s^2}{\omega_{n_{sp}}^2}+\frac{2\zeta_{sp}}{\omega_{n_{sp}}}s+1\right)}$$

or

$$\frac{\theta}{F_s} = \frac{K_\theta(\tau_{\theta_2}s+1)}{s\left(\frac{s^2}{\omega_{n_{sp}}^2}+\frac{2\zeta_{sp}}{\omega_{n_{sp}}}s+1\right)}$$

where

$$K_\theta = \frac{M_{F_s}}{\omega_{n_{sp}}^2\tau_{\theta_2}} = \frac{g}{V_T(F_s/n)_{SS}}$$

Note: K_θ as defined above is the same as the steady-state value of q/F_s